AAS 21-248

PROCESS NOISE COVARIANCE MODELING FOR ABSOLUTE AND RELATIVE ORBIT DETERMINATION

Nathan Stacey[*], **Simone D'Amico**[†]

This paper develops new analytical process noise covariance models for both absolute and relative orbit determination in a discrete-time Kalman filtering framework. Process noise is always present in orbit determination due to dynamics modeling deficiencies, and accurately modeling this noise is essential for optimal estimation. A common approach called state noise compensation models process noise as zero-mean Gaussian white noise accelerations. The resulting process noise covariance can be evaluated numerically, which is computationally intensive, or through a widely used analytical model that is restricted to a Cartesian state and small propagation intervals. Moreover, mathematically rigorous, analytical process noise covariance models for relative spacecraft states are not currently available. To address these limitations of the state of the art, new analytical process noise covariance models are developed for state noise compensation for both Cartesian and orbital element state representations. Two frameworks are then presented for modeling the process noise covariance of relative spacecraft states by assuming either small or large interspacecraft separations. The presented techniques are validated through numerical simulations.

INTRODUCTION

In Kalman filtering, process noise represents deviations of the true dynamics from the modeled dynamics. Process noise is always present in orbit determination due to imperfect knowledge of the numerous complex forces acting on a spacecraft and limited computational resources for modeling those forces. Computational capabilities are especially constrained for onboard orbit determination, often necessitating reduced order dynamics models. Accurately capturing dynamics modeling deficiencies through process noise is essential for optimal estimation. Inaccurate process noise modeling increases estimation error and can result in filter inconsistency and divergence.[1,2] Modeling process noise is also critical for satellite conjunction analysis. In particular, analytical process noise models are advantageous because they are computationally efficient and provide insight into system behavior. This paper addresses gaps in the state of the art through the development of new analytical process noise covariance models for absolute and relative spacecraft states parameterized using both Cartesian coordinates and orbital elements.

A variety of approaches have been established to model the effects on the spacecraft state error covariance due to unmodeled accelerations, which are the difference between the true and modeled spacecraft accelerations. A common ad hoc method is to manually tune a diagonal process noise covariance. Such an approach does not scale the process noise covariance according to the length of the propagation interval, so the covariance must be retuned for different propagation interval lengths.[3] Furthermore, this technique does not capture the cross-covariance between elements of the spacecraft state, and does not provide any dynamical consistency between the magnitudes of the process noise covariance of the different spacecraft state components. A second approach considers the effects of auto-correlated central body gravity modeling errors of both commission and omission.[4,5] However, these models are rarely used onboard due to computational cost.[3] Furthermore, this method cannot be used for uncertainties in other types of spacecraft accelerations

[*]Doctoral Candidate, Stanford University, Department of Aeronautics and Astronautics, Space Rendezvous Laboratory, Durand Building, 496 Lomita Mall, Stanford, CA 94305-4035, Student Member AIAA.

[†]Associate Professor, Stanford University, Department of Aeronautics and Astronautics, Space Rendezvous Laboratory, Durand Building, 496 Lomita Mall, Stanford, CA 94305-4035, Member AIAA.

such as drag, solar radiation pressure, and third body effects. The process noise due to maneuver execution errors can also be explicitly modeled.[3,6] Another approach called dynamic model compensation directly estimates the unmodeled accelerations by augmenting the estimated state vector with empirical accelerations.[7–11] Augmenting the state vector increases filter computation time, and the performance of dynamic model compensation depends on the tuning of parameters in the dynamical model of the empirical accelerations such as the empirical acceleration time correlation constants.[9,12]

Advances in process noise modeling have primarily focused on an absolute Cartesian spacecraft state. However, the most appropriate state representation depends on the application. The spacecraft state can be parameterized as absolute or relative Cartesian coordinates as well as absolute or relative orbital elements. An absolute state describes the motion of a single spacecraft. In contrast, a relative state is a function of the absolute states of two spacecraft and describes the motion of one spacecraft relative to the other. Cartesian coordinates are most frequently used because of their more direct relation to the modeled measurements and because they do not have any singularities. Although orbital element states suffer from singularities, they have several advantages over Cartesian coordinates. Since most orbital elements vary more slowly in time than position and velocity, orbital elements can often be numerically integrated more efficiently.[13] Orbital elements also enable analytical perturbation models[14,15] and provide greater geometric insight than a Cartesian state. See Hintz[16] and Sullivan et al.[17] for comprehensive reviews of absolute and relative state parameterizations respectively. See Carpenter et al.[3] for the tradeoffs involved in orbit determination when parameterizing the state of a second spacecraft as either an absolute or relative state.

One of the most widely used process noise models in orbit determination is state noise compensation (SNC).[3,7,18,19] Although the unmodeled accelerations are generally correlated in time, SNC treats the unmodeled accelerations as zero-mean Gaussian white process noise. The resulting process noise covariance can be evaluated through numerical integration, which is computationally intensive. Alternatively, an analytical SNC model is commonly used that assumes zero nominal spacecraft acceleration. However, this model is restricted to an absolute Cartesian state and is only valid for small propagation intervals.[3,18,19] The authors are not aware of analytical SNC models for orbital element state representations or mathematically rigorous, analytical process noise covariance models for relative spacecraft states.

To overcome these limitations, this paper develops new analytical SNC process noise covariance models for both absolute and relative spacecraft states. The following section reviews relevant background information on SNC and relative motion dynamical modeling. The subsequent section develops process noise covariance models for absolute Cartesian and orbital element states by assuming either a circular orbit or a small propagation interval. The next two sections present frameworks for modeling the process noise covariance of relative spacecraft states by assuming either small or large interspacecraft separations. The presented models are validated through numerical simulations in the penultimate section. Finally, conclusions are provided based on the numerical results.

BACKGROUND

State Noise Compensation for an Absolute Spacecraft State

Let $\boldsymbol{x}_\alpha(t) \in \mathbb{R}^6$ denote the absolute state of a spacecraft parameterized in either Cartesian coordinates or a set of orbital elements. The specific state representation is indicated by the subscript α. The mean state estimate at time step i after processing all the measurements through time step j is $\hat{\boldsymbol{x}}_{\alpha,i|j}$. Assuming an unbiased estimator such that $\mathrm{E}[\hat{\boldsymbol{x}}_{\alpha,i|j}] = \boldsymbol{x}_\alpha(t_i)$, the error covariance or formal covariance of the mean state estimate at time step i after processing all the measurements through time step j is $\mathbf{P}_{\alpha,i|j} = \mathrm{E}[(\boldsymbol{x}_\alpha(t_i) - \hat{\boldsymbol{x}}_{\alpha,i|j})(\boldsymbol{x}_\alpha(t_i) - \hat{\boldsymbol{x}}_{\alpha,i|j})^T]$. An essential task in sequential orbit determination as well as satellite conjunction analysis is to propagate the error covariance to some future time t_k, which involves determining $\mathbf{P}_{\alpha,k|k-1}$ given $\hat{\boldsymbol{x}}_{\alpha,k-1|k-1}$ and $\mathbf{P}_{\alpha,k-1|k-1}$.

In general, the dynamical model of the spacecraft state is given by some nonlinear function $\dot{\boldsymbol{x}}_\alpha(t) = \boldsymbol{f}(\boldsymbol{x}_\alpha(t), \boldsymbol{u}(t), t)$ where $\boldsymbol{u}(t)$ is the control input. The approach taken in an extended Kalman filtering framework is to linearize the dynamical model over the propagation interval $[t_{k-1}, t_k]$ about the mean state estimate taking into account all measurements through time t_{k-1}. This linearization results in a linear time-varying

system

$$\dot{\boldsymbol{X}}_\alpha(t) = \mathbf{A}_\alpha(t)\boldsymbol{X}_\alpha(t) + \mathbf{B}_\alpha(t)\boldsymbol{u}(t) + \boldsymbol{\Gamma}_\alpha(t)\boldsymbol{\epsilon}(t) \tag{1}$$

where $\boldsymbol{X}_\alpha(t) = \boldsymbol{x}_\alpha(t) - \hat{\boldsymbol{x}}_\alpha(t)$ is the state estimate error, and $\hat{\boldsymbol{x}}_\alpha(t)$ is the mean state estimate at time t taking into account all measurements through time t_{k-1} such that $\hat{\boldsymbol{x}}_\alpha(t_k) = \hat{\boldsymbol{x}}_{\alpha,k|k-1}$. Here $\mathbf{A}_\alpha$ is the plant matrix, $\mathbf{B}_\alpha$ is the control input matrix, and $\boldsymbol{\Gamma}_\alpha$ is the process noise mapping matrix. These matrices are defined by the partial derivatives

$$\mathbf{A}_\alpha(t) = \frac{\partial \dot{\boldsymbol{x}}_\alpha(t)}{\partial \boldsymbol{x}_\alpha(t)}, \qquad \mathbf{B}_\alpha(t) = \frac{\partial \dot{\boldsymbol{x}}_\alpha(t)}{\partial \boldsymbol{u}(t)}, \qquad \boldsymbol{\Gamma}_\alpha(t) = \frac{\partial \dot{\boldsymbol{x}}_\alpha(t)}{\partial \boldsymbol{\epsilon}(t)} \tag{2}$$

evaluated at the mean state estimate $\hat{\boldsymbol{x}}_\alpha(t)$.

The continuous-time process noise $\boldsymbol{\epsilon}$ describes stochastic deviations from the nominal spacecraft dynamics. If the dynamics were truly linear, the only sources of process noise would be numerical error and unmodeled accelerations. Thus, throughout this paper $\boldsymbol{\epsilon}$ physically represents unmodeled accelerations since they generally create orders of magnitude more process noise than numerical error. Here $\boldsymbol{\epsilon} \in \mathbb{R}^3$ is modeled as a zero-mean white Gaussian process with autocovariance

$$\mathrm{E}[\boldsymbol{\epsilon}(t)\boldsymbol{\epsilon}(\tau)^T] = \widetilde{\mathbf{Q}}\delta(t-\tau) \tag{3}$$

where $\delta(\cdot)$ is the Dirac delta function and $\widetilde{\mathbf{Q}} \in \mathbb{R}^{3\times 3}$ is the process noise power spectral density, which describes the strength of the unmodeled accelerations. This approach to process noise modeling is called SNC.[3,7] The stochastic vector of unmodeled accelerations $\boldsymbol{\epsilon}$ can be inertial or radial-transverse-normal (RTN) coordinates, which will be denoted by the superscripts $\mathcal{I}$ and $\mathcal{R}$ respectively. Thus $\boldsymbol{\epsilon}^{\mathcal{I}}(t) = {}_{\mathcal{R}\to\mathcal{I}}\mathbf{R}(t)\boldsymbol{\epsilon}^{\mathcal{R}}(t)$ where ${}_{\mathcal{R}\to\mathcal{I}}\mathbf{R}(\mathrm{t}) \in \mathbb{R}^{3\times 3}$ is the rotation matrix from the RTN frame to the inertial frame at time t. The power spectral density of $\boldsymbol{\epsilon}^{\mathcal{I}}$ and $\boldsymbol{\epsilon}^{\mathcal{R}}$ are $\widetilde{\mathbf{Q}}^{\mathcal{I}}$ and $\widetilde{\mathbf{Q}}^{\mathcal{R}}$ respectively. In the RTN frame, also referred to as the Hill frame, the radial and normal axes are aligned with the chief spacecraft position and angular momentum vectors respectively. The transverse axis completes the right-handed triad and is positive in the direction of the chief velocity. Typically, the spacecraft dynamics are highly nonlinear, and $\widetilde{\mathbf{Q}}$ should be large enough to also accommodate errors due to dynamical nonlinearities in the propagation of the mean state estimate and associated error covariance.

The discrete-time solution of Eq. (1) is

$$\boldsymbol{X}_\alpha(t_k) = \boldsymbol{\Phi}_\alpha(t_k, t_{k-1})\boldsymbol{X}_\alpha(t_{k-1}) + \int_{t_{k-1}}^{t_k} \boldsymbol{\Phi}_\alpha(t_k,\tau)\mathbf{B}_\alpha(\tau)\boldsymbol{u}(\tau)d\tau + \boldsymbol{w}_{\alpha,k} \tag{4}$$

where the Jacobian $\boldsymbol{\Phi}_\alpha(t_k, t_{k-1}) = \frac{\partial \boldsymbol{x}_\alpha(t_k)}{\partial \boldsymbol{x}_\alpha(t_{k-1})}$ evaluated at the mean state estimate is the state transition matrix. The discrete-time process noise is $\boldsymbol{w}_{\alpha,k} \sim \mathcal{N}(\mathbf{0}, \mathbf{Q}_{\alpha,k})$, and the process noise covariance is

$$\mathbf{Q}_{\alpha,k} = \int_{t_{k-1}}^{t_k} \boldsymbol{\Phi}_\alpha(t_k,\tau)\boldsymbol{\Gamma}_\alpha(\tau)\widetilde{\mathbf{Q}}\boldsymbol{\Gamma}_\alpha(\tau)^T\boldsymbol{\Phi}_\alpha(t_k,\tau)^T d\tau \tag{5}$$

Due to the structure of Eq. (5), $\mathbf{Q}_{\alpha,k}$ is guaranteed symmetric and positive semi-definite provided that $\widetilde{\mathbf{Q}}$ is symmetric and positive semi-definite. The propagated or time-updated error covariance is

$$\mathbf{P}_{\alpha,k|k-1} = \mathrm{E}[\boldsymbol{X}_\alpha(t_k)\boldsymbol{X}_\alpha(t_k)^T] \tag{6}$$

$$= \boldsymbol{\Phi}_{\alpha,k}\mathbf{P}_{\alpha,k-1|k-1}\boldsymbol{\Phi}_{\alpha,k}^T + \mathbf{Q}_{\alpha,k} \tag{7}$$

where $\boldsymbol{\Phi}_{\alpha,k} = \boldsymbol{\Phi}_\alpha(t_k, t_{k-1})$.

The process noise covariance integral in Eq. (5) can be evaluated numerically provided that the state transition matrix and process noise mapping matrix are integrable functions. However, analytical solutions

are desirable because they significantly reduce computation time and provide insight into system behavior. One common analytical approximation of Eq. (5) considers an absolute, inertial Cartesian state

$$\boldsymbol{x}_{\mathcal{I}} = \begin{bmatrix} \boldsymbol{r} \\ \boldsymbol{v} \end{bmatrix} \tag{8}$$

where $\boldsymbol{r}$ and $\boldsymbol{v}$ are the inertial position and velocity vectors respectively. Assuming kinematic motion where the nominal spacecraft acceleration is zero,

$$\boldsymbol{\Phi}_{\mathcal{I}}(t_k, t_{k-1}) = \begin{bmatrix} \mathbf{I}_{3\times3} & \Delta t_k \mathbf{I}_{3\times3} \\ \mathbf{0}_{3\times3} & \mathbf{I}_{3\times3} \end{bmatrix} \tag{9}$$

where $\Delta t_k = t_k - t_{k-1}$ is the length of the propagation interval $[t_{k-1}, t_k]$. The identity matrix and matrix of zeros with three rows and columns are $\mathbf{I}_{3\times3}$ and $\mathbf{0}_{3\times3}$ respectively. Modeling $\boldsymbol{\epsilon}$ in the inertial frame, the process noise mapping matrix is

$$\boldsymbol{\Gamma}_{\mathcal{I}} = \begin{bmatrix} \mathbf{0}_{3\times3} \\ \mathbf{I}_{3\times3} \end{bmatrix} \tag{10}$$

Substituting Eqs. (9-10) and $\widetilde{\mathbf{Q}} = \widetilde{\mathbf{Q}}^{\mathcal{I}}$ into Eq. (5) and evaluating the integral yields[3,19]

$$\mathbf{Q}_{\mathcal{I},k} = \begin{bmatrix} \frac{1}{3}\Delta t_k^3 \widetilde{\mathbf{Q}}^{\mathcal{I}} & \frac{1}{2}\Delta t_k^2 \widetilde{\mathbf{Q}}^{\mathcal{I}} \\ \frac{1}{2}\Delta t_k^2 \widetilde{\mathbf{Q}}^{\mathcal{I}} & \Delta t_k \widetilde{\mathbf{Q}}^{\mathcal{I}} \end{bmatrix} \tag{11}$$

Assuming the orientation of the RTN frame relative to the inertial frame is constant over a small propagation interval $[t_{k-1}, t_k]$, the relation $\widetilde{\mathbf{Q}}^{\mathcal{I}} = \underset{\mathcal{R}\to\mathcal{I}}{\mathbf{R}} \widetilde{\mathbf{Q}}^{\mathcal{R}} \underset{\mathcal{R}\to\mathcal{I}}{\mathbf{R}}^T$ can be substituted into Eq. (11).[3] Another approach to simplify Eq. (5) is to model $\boldsymbol{\epsilon}$ as constant over the interval $[t_{k-1}, t_k]$.[7] However, the covariance of $\boldsymbol{\epsilon}$ must then be retuned for different propagation interval lengths as observed by Carpenter et. al.[3] Although the analytical process noise covariance model in Eq. (11) is widely used, it is only valid for small propagation intervals.[3] Furthermore, the authors are not aware of any analytical SNC models for orbital element states or mathematically rigorous, analytical process noise covariance models for relative spacecraft states. These gaps in the state of the art are addressed in this paper.

Hill-Clohessy-Wiltshire Equations

This section reviews the Hill-Clohessy-Wiltshire (HCW) equations,[20] which can be parameterized in rectilinear or curvilinear coordinates, and the corresponding discrete-time solution.[21,22] The solution of the HCW equations was used by Geller[23] to approximate a scalar metric of the uncertainty of the position of one spacecraft relative to another spacecraft due to navigation and maneuver execution errors as well as umodeled accelerations. In the following sections, the solution of the HCW equations is used for the first time to construct an analytical model of the full process noise covariance of both absolute and relative Cartesian states.

Throughout this paper, $\delta\boldsymbol{x}_\alpha(t) \in \mathbb{R}^6$ denotes a relative spacecraft state where the specific relative state representation is denoted by the subscript α. Let

$$\delta\boldsymbol{x}_{\mathcal{R}} = \begin{bmatrix} \delta\boldsymbol{r} \\ \delta\boldsymbol{v} \end{bmatrix} = \begin{bmatrix} \underset{\mathcal{I}\to\mathcal{R}}{\mathbf{R}}(\boldsymbol{r}_d - \boldsymbol{r}_c) \\ \underset{\mathcal{I}\to\mathcal{R}}{\mathbf{R}}(\boldsymbol{v}_d - \boldsymbol{v}_c) - \boldsymbol{w}^{\times} \underset{\mathcal{I}\to\mathcal{R}}{\mathbf{R}}(\boldsymbol{r}_d - \boldsymbol{r}_c) \end{bmatrix} \tag{12}$$

be the state of a deputy spacecraft relative to a chief expressed in the chief RTN frame. The inertial Cartesian coordinates, defined in Eq. (8), of the chief and deputy are denoted by the subscripts c and d respectively. The chief orbit may be the orbit of either a physical or virtual spacecraft. Notice that for the relative velocity vector $\delta\boldsymbol{v}$, the time derivative has been taken in the chief RTN frame. Here $\delta\boldsymbol{r} = [\delta r_r \quad \delta r_t \quad \delta r_n]^T$ and $\delta\boldsymbol{v} = [\delta v_r \quad \delta v_t \quad \delta v_n]^T$. The angular velocity vector of the chief RTN frame with respect to the inertial

frame expressed in the chief RTN frame is denoted $\boldsymbol{w}$. The cross product matrix of $\boldsymbol{w}$ is $\boldsymbol{w}^{\times}$, which is a skew-symmetric matrix defined such that

$$\boldsymbol{w} = \begin{bmatrix} w_r \\ w_t \\ w_n \end{bmatrix} \implies \boldsymbol{w}^{\times} = \begin{bmatrix} 0 & -w_n & w_t \\ w_n & 0 & -w_r \\ -w_t & w_r & 0 \end{bmatrix} \tag{13}$$

For two-body motion, $w_r = w_t = 0$ and $w_n = \dot{\theta}_c$ where $\dot{\theta}_c$ is the time rate of change of the angle between the chief position vector $\boldsymbol{r}_c$ and an arbitrary fixed vector in the chief orbital plane.

Consider the spherical coordinates

$$\rho = ((r_c + \delta r_r)^2 + \delta r_t^2 + \delta r_n^2)^{1/2} - r_c \tag{14}$$

$$\theta = \text{atan}\left(\frac{\delta r_t}{r_c + \delta r_r}\right) \tag{15}$$

$$\phi = \text{atan}\left(\frac{\delta r_n}{((r_c + \delta r_r)^2 + \delta r_t^2)^{1/2}}\right) \tag{16}$$

where $r_c = ||\boldsymbol{r}_c||$. Here $\rho = ||\boldsymbol{r}_d|| - r_c$, θ is the angle between the projection of the deputy position vector onto the chief orbital plane and the chief position vector, and ϕ is the angle between the deputy position vector and its projection onto the chief orbital plane. The angles θ and ϕ are measured positive in the directions of the chief velocity and angular momentum vectors respectively as shown in Fig. 1. The nonlinear equations of relative motion parameterized using ρ, θ, and ϕ are derived by Willis et al.[24] considering only two-body motion. Linearizing these equations about zero interspacecraft separation, assuming a circular chief orbit, and including differential perturbing accelerations yields[21,24]

$$\ddot{\rho} = 3n^2\rho + 2nr_c\dot{\theta} + \delta d_r \tag{17}$$

$$r_c\ddot{\theta} = -2n\dot{\rho} + \delta d_t \tag{18}$$

$$r_c\ddot{\phi} = -n^2 r_c\phi + \delta d_n \tag{19}$$

The chief mean motion is denoted n, and $\delta\boldsymbol{d} = \boldsymbol{d}_d - \boldsymbol{d}_c = [\delta d_r \;\; \delta d_t \;\; \delta d_n]^T$ is the difference between the perturbing accelerations of the deputy and chief expressed in the chief RTN frame.

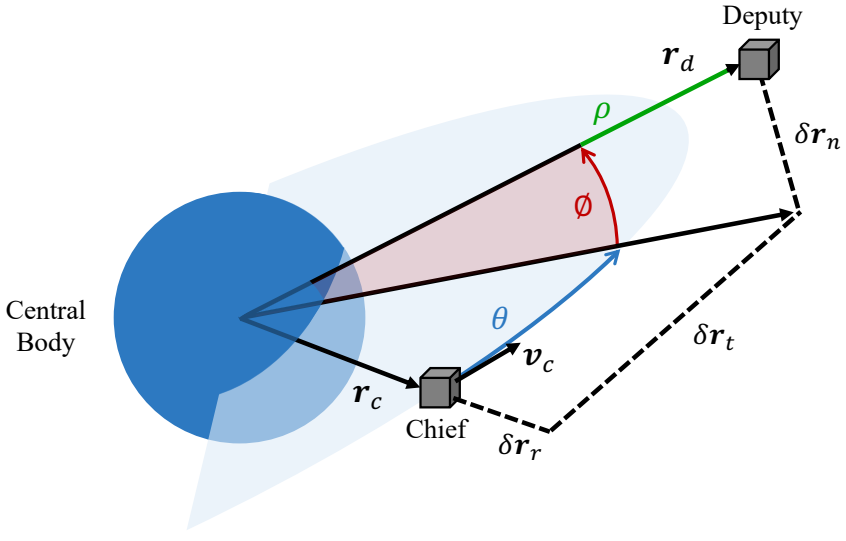

Figure 1: Rectilinear and curvilinear relative spacecraft coordinates.

One particular curvilinear relative state is

$$\delta\boldsymbol{x}_\psi = [\rho \;\; r_c\theta \;\; r_c\phi \;\; \dot{\rho} \;\; r_c\dot{\theta} \;\; r_c\dot{\phi}]^T \tag{20}$$

The discrete-time solution of Eqs. (17-19) yields the state transition matrix

$$\boldsymbol{\Phi}_{\delta\psi}(t,0) = \begin{bmatrix} 4-3\cos nt & 0 & 0 & \frac{1}{n}\sin nt & \frac{2}{n}(1-\cos nt) & 0 \\ 6(\sin nt - nt) & 1 & 0 & \frac{2}{n}(\cos nt - 1) & \frac{1}{n}(4\sin nt - 3nt) & 0 \\ 0 & 0 & \cos nt & 0 & 0 & \frac{1}{n}\sin nt \\ 3n\sin nt & 0 & 0 & \cos nt & 2\sin nt & 0 \\ 6n(\cos nt - 1) & 0 & 0 & -2\sin nt & 4\cos nt - 3 & 0 \\ 0 & 0 & -n\sin nt & 0 & 0 & \cos nt \end{bmatrix} \tag{21}$$

that propagates $\delta\boldsymbol{x}_\psi$ from time 0 to t, which is the well-known solution of the HCW equations. The HCW equations can also be parameterized in the rectilinear coordinates $\delta\boldsymbol{x}_\mathcal{R}$ defined in Eq. (12), and the corresponding state transition matrix is identical to that shown in Eq. (21). Parameterizing the state in curvilinear coordinates instead of rectilinear coordinates has been shown to reduce errors incurred by the linearization when using the state transition matrix to propagate the relative state.[21,22]

ABSOLUTE PROCESS NOISE COVARIANCE MODELING

In general, it is difficult to obtain an exact analytical solution of the integral in Eq. (5) that is reasonably concise even when only considering two-body motion. For a Cartesian state, the complexity of the integral in Eq. (5) is principally due to the state transition matrix. As a result, a concise analytical approximation of Eq. (5) is obtained for a Cartesian state by simplifying the state transition matrix through the assumption of a circular orbit. In contrast, for an orbital element state the complexity of the integral in Eq. (5) is primarily due to the process noise mapping matrix, which is given by the Gauss Variational Equations. An approximation of Eq. (5) for orbital element states is derived by simplifying the process noise mapping matrix through the assumption of either a circular orbit or a short propagation interval.

Typically, it is advantageous to model spacecraft acceleration uncertainty in the RTN frame since the amount of acceleration uncertainty in each axis of the RTN frame generally varies less than in each axis of an inertial frame. For example, consider a case where atmospheric drag is the largest contributor to spacecraft acceleration uncertainty. Throughout the orbit, the acceleration uncertainty is consistently large in the along-track direction and relatively small in the radial and normal directions. In contrast, the level of acceleration uncertainty in each axis of an inertial frame will change significantly throughout the orbit. Consequently, the unmodeled acceleration power spectral density, $\widetilde{\mathbf{Q}}$, will be modeled in the RTN frame throughout the rest of this paper. For simplicity, it is assumed that the power spectral density matrix is diagonal such that

$$\widetilde{\mathbf{Q}}^\mathcal{R} = \begin{bmatrix} \widetilde{Q}_r & 0 & 0 \\ 0 & \widetilde{Q}_t & 0 \\ 0 & 0 & \widetilde{Q}_n \end{bmatrix} \tag{22}$$

Here $\widetilde{Q}_r$, $\widetilde{Q}_t$, and $\widetilde{Q}_n$ describe the strength of the unmodeled accelerations in the radial, transverse, and normal directions respectively. A diagonal $\widetilde{\mathbf{Q}}^\mathcal{R}$ enables the expression for $\mathbf{Q}_{\alpha,k}$ in Eq. (5) to be written as

$$\mathbf{Q}_{\alpha,k} = \mathbf{Q}^r_{\alpha,k} + \mathbf{Q}^t_{\alpha,k} + \mathbf{Q}^n_{\alpha,k} \tag{23}$$

Here

$$\mathbf{Q}^i_{\alpha,k} = \widetilde{Q}_i \int_{t_{k-1}}^{t_k} \overline{\boldsymbol{\Gamma}}_{\alpha,i}(t_k,\tau)\overline{\boldsymbol{\Gamma}}_{\alpha,i}(t_k,\tau)^T d\tau \tag{24}$$

is the contribution to $\mathbf{Q}_{\alpha,k}$ due to unmodeled accelerations in axis i of the RTN frame where $i \in \{r,t,n\}$. The vectors $\overline{\boldsymbol{\Gamma}}_{\alpha,r}(t_k,\tau)$, $\overline{\boldsymbol{\Gamma}}_{\alpha,t}(t_k,\tau)$, and $\overline{\boldsymbol{\Gamma}}_{\alpha,n}(t_k,\tau)$ are the first, second, and third columns respectively of

$$\overline{\boldsymbol{\Gamma}}_\alpha(t_k,\tau) = \boldsymbol{\Phi}_\alpha(t_k,\tau)\boldsymbol{\Gamma}_\alpha(\tau) \tag{25}$$

The particular values of $\widetilde{Q}_r$, $\widetilde{Q}_t$, and $\widetilde{Q}_n$ are based on a priori knowledge of the dynamical environment. For example, these values can be selected in order to match elements of $\mathbf{Q}_{\alpha,k}$ to corresponding estimates[19] or in order for the filter error covariance to match an empirical approximation of the true error covariance.[3]

Cartesian State and Circular Orbit

This section leverages the solution of the HCW equations to develop a process noise covariance model for the absolute, inertial Cartesian state of a spacecraft $\boldsymbol{x}_{\mathcal{I}}$ for near-circular orbits considering only two-body motion. The state error of an inertial Cartesian state $\boldsymbol{X}_{\mathcal{I}}(t) = \boldsymbol{x}_{\mathcal{I}}(t) - \hat{\boldsymbol{x}}_{\mathcal{I}}(t)$ can be thought of as the state of a deputy relative to a chief spacecraft. The deputy is the true spacecraft state $\boldsymbol{x}_{\mathcal{I}}$, and the chief is the estimated state $\hat{\boldsymbol{x}}_{\mathcal{I}}$, which is a virtual orbit. This relative motion is described in a linearized framework through Eqs. (1) and (4). The relative motion can be equivalently parameterized using the curvilinear state $\delta\boldsymbol{x}_{\psi}$ defined in Eq. (20). The parameterization of $\boldsymbol{X}_{\mathcal{I}}$ in curvilinear coordinates will be denoted $\delta\boldsymbol{X}_{\psi}$. Assuming an unbiased estimator, the expectation of the estimate error is zero. In other words, $\mathrm{E}[\delta\boldsymbol{X}_{\psi}(t)] = \mathbf{0}$. The dynamics of $\delta\boldsymbol{X}_{\psi}$ can be linearized about $\delta\boldsymbol{X}_{\psi} = \mathbf{0}$, resulting in a linear time-varying system similar to Eq. (1). Following the same approach used to derive Eqs. (4-7), the covariance of $\delta\boldsymbol{X}_{\psi}$ is

$$\mathbf{P}_{\psi,k|k-1} = \mathrm{E}[\delta\boldsymbol{X}_{\psi}(t_k)\delta\boldsymbol{X}_{\psi}(t_k)^T] \tag{26}$$

$$= \mathbf{\Phi}_{\psi,k}\mathbf{P}_{\psi,k-1|k-1}\mathbf{\Phi}_{\psi,k}^T + \mathbf{Q}_{\psi,k} \tag{27}$$

Here $\mathbf{\Phi}_{\psi,k}$ is the state transition matrix of $\delta\boldsymbol{X}_{\psi}$. Assuming two-body motion and a circular orbit, $\mathbf{\Phi}_{\psi,k}$ is equivalent to Eq. (21). In this case, n in Eq. (21) refers to the mean motion computed from the mean state estimate. The unmodeled accelerations $\boldsymbol{\epsilon}$ are modeled in the RTN frame of the estimated trajectory. The process noise mapping matrix is then deduced from Eqs. (17-19) to be

$$\mathbf{\Gamma}_{\psi} = \begin{bmatrix} \mathbf{0}_{3\times3} \\ \mathbf{I}_{3\times3} \end{bmatrix} \tag{28}$$

The matrix $\mathbf{Q}_{\psi,k}$ is obtained by substituting Eqs. (21-22) and Eq. (28) into Eq. (5). The solution to Eq. (5) is computed by evaluating Eq. (24) and substituting the result into Eq. (23). Analytically evaluating Eq. (24) for each axis yields

$$\mathbf{Q}^r_{\psi,k} = \widetilde{Q}_r \begin{bmatrix} \frac{1}{n^2}\zeta_{ss} & \ddots & \ddots & \ddots & \ddots & \ddots \\ \frac{2}{n^2}(\zeta_{cs}-\zeta_s) & \frac{4}{n^2}(\zeta_{cc}-2\zeta_c+\Delta t_k) & \ddots & \ddots & \ddots & \ddots \\ 0 & 0 & 0 & \ddots & \ddots & \ddots \\ \frac{1}{n}\zeta_{cs} & \frac{2}{n}(\zeta_{cc}-\zeta_c) & 0 & \zeta_{cc} & \ddots & \ddots \\ \frac{-2}{n}\zeta_{ss} & \frac{-4}{n}(\zeta_{cs}-\zeta_s) & 0 & -2\zeta_{cs} & 4\zeta_{ss} & \ddots \\ 0 & 0 & 0 & 0 & 0 & 0 \end{bmatrix} \tag{29}$$

$$\mathbf{Q}^n_{\psi,k} = \widetilde{Q}_n \begin{bmatrix} 0 & \ddots & \ddots & \ddots & \ddots & \ddots \\ 0 & 0 & \ddots & \ddots & \ddots & \ddots \\ 0 & 0 & \frac{1}{n^2}\zeta_{ss} & \ddots & \ddots & \ddots \\ 0 & 0 & 0 & 0 & \ddots & \ddots \\ 0 & 0 & 0 & 0 & 0 & \ddots \\ 0 & 0 & \frac{1}{n}\zeta_{cs} & 0 & 0 & \zeta_{cc} \end{bmatrix} \tag{30}$$

$$\mathbf{Q}^t_{\psi,k} = \widetilde{Q}_t \begin{bmatrix} \frac{4}{n^2}(\Delta t_k + \zeta_{cc} - 2\zeta_c) & \ddots & \ddots \\ \frac{2}{n^2}(3n\zeta_{tc} - 4\zeta_{cs} + 4\zeta_s - \frac{3n}{2}\Delta t_k^2) & \frac{1}{n^2}(3n^2\Delta t_k^3 + 16\zeta_{ss} - 24n\zeta_{ts}) & \ddots \\ 0 & 0 & 0 \\ \frac{4}{n}(\zeta_s - \zeta_{cs}) & \frac{2}{n}(4\zeta_{ss} - 3n\zeta_{ts}) & 0 \\ \frac{2}{n}(7\zeta_c - 4\zeta_{cc} - 3\Delta t_k) & \frac{1}{n}(16\zeta_{cs} - 12n\zeta_{tc} - 12\zeta_s + \frac{9n}{2}\Delta t_k^2) & 0 \\ 0 & 0 & 0 \end{bmatrix}$$

$$\begin{bmatrix} \ddots & \ddots & \ddots \\ \ddots & \ddots & \ddots \\ \ddots & \ddots & \ddots \\ 4\zeta_{ss} & \ddots & \ddots \\ 8\zeta_{cs} - 6\zeta_s & 9\Delta t_k + 16\zeta_{cc} - 24\zeta_c & \ddots \\ 0 & 0 & 0 \end{bmatrix} \tag{31}$$

with the auxiliary variables

$$\begin{aligned} \zeta_c &= \int_{t_{k-1}}^{t_k} \cos(n(t_k - \tau))\, d\tau = \frac{1}{n}\sin n\Delta t_k \\ \zeta_s &= \int_{t_{k-1}}^{t_k} \sin(n(t_k - \tau))\, d\tau = \frac{1}{n}(1 - \cos n\Delta t_k) \\ \zeta_{cc} &= \int_{t_{k-1}}^{t_k} \cos^2(n(t_k - \tau))\, d\tau = \frac{\Delta t_k}{2} + \frac{1}{4n}\sin 2n\Delta t_k \\ \zeta_{ss} &= \int_{t_{k-1}}^{t_k} \sin^2(n(t_k - \tau))\, d\tau = \frac{\Delta t_k}{2} - \frac{1}{4n}\sin 2n\Delta t_k \\ \zeta_{cs} &= \int_{t_{k-1}}^{t_k} \cos(n(t_k - \tau))\sin(n(t_k - \tau))\, d\tau = \frac{1}{4n}(1 - \cos 2n\Delta t_k) \\ \zeta_{tc} &= \int_{t_{k-1}}^{t_k} (t_k - \tau)\cos(n(t_k - \tau))\, d\tau = \frac{1}{n^2}(\cos n\Delta t_k - 1) + \frac{\Delta t_k}{n}\sin n\Delta t_k \\ \zeta_{ts} &= \int_{t_{k-1}}^{t_k} (t_k - \tau)\sin(n(t_k - \tau))\, d\tau = \frac{-\Delta t_k}{n}\cos n\Delta t_k + \frac{1}{n^2}\sin n\Delta t_k \end{aligned} \tag{32}$$

Each matrix in Eqs. (29-31) is symmetric, and only the unique elements in the lower triangular portion of each matrix are specified for conciseness.

Recalling the assumption of an unbiased filter such that $\mathrm{E}[\boldsymbol{X}_{\mathcal{I}}(t_k)] = \mathrm{E}[\delta\boldsymbol{X}_{\psi}(t_k)] = \mathbf{0}$, $\boldsymbol{X}_{\mathcal{I}}(t_k)$ can be written in terms of its curvilinear parameterization through a first-order Taylor series expansion about $\boldsymbol{X}_{\mathcal{I}}(t_k) = \mathbf{0}$ as

$$\boldsymbol{X}_{\mathcal{I}}(t_k) = \mathbf{J}_{\mathcal{I}\psi}(t_k)\delta\boldsymbol{X}_{\psi}(t_k) \tag{33}$$

where

$$\mathbf{J}_{\mathcal{I}\psi}(t_k) = \left.\frac{\partial\delta\boldsymbol{x}_{\mathcal{I}}(t_k)}{\partial\delta\boldsymbol{x}_{\psi}(t_k)}\right|_{\delta\boldsymbol{x}_{\psi}=\mathbf{0}} \tag{34}$$

Here $\delta\boldsymbol{x}_{\mathcal{I}} = \boldsymbol{x}^d_{\mathcal{I}} - \boldsymbol{x}^c_{\mathcal{I}}$ is the difference between the absolute, inertial Cartesian states of a deputy and chief. Eq. (34) can be expanded using the chain rule as

$$\mathbf{J}_{\mathcal{I}\psi}(t_k) = \left(\left.\frac{\partial\delta\boldsymbol{x}_{\mathcal{I}}(t_k)}{\partial\,\delta\boldsymbol{x}_{\mathcal{R}}(t_k)}\right|_{\delta\boldsymbol{x}_{\mathcal{R}}(t_k)=\mathbf{0}}\right)\left(\left.\frac{\partial\,\delta\boldsymbol{x}_{\mathcal{R}}(t_k)}{\partial\,\delta\boldsymbol{x}_{\psi}(t_k)}\right|_{\delta\boldsymbol{x}_{\psi}(t_k)=\mathbf{0}}\right) \tag{35}$$

The first matrix of partial derivatives in Eq. (35) is deduced from Eq. (12) to be

$$\left.\frac{\partial \delta \boldsymbol{x}_{\mathcal{I}}(t_k)}{\partial\, \delta \boldsymbol{x}_{\mathcal{R}}(t_k)}\right|_{\delta \boldsymbol{x}_{\mathcal{R}}(t_k)=\mathbf{0}} = \begin{bmatrix} \underset{\mathcal{R}\to\mathcal{I}}{\mathbf{R}}(t_k) & \mathbf{0}_{3\times 3} \\ \underset{\mathcal{R}\to\mathcal{I}}{\mathbf{R}}(t_k)\boldsymbol{w}^{\times} & \underset{\mathcal{R}\to\mathcal{I}}{\mathbf{R}}(t_k) \end{bmatrix} \tag{36}$$

Since the relative Cartesian and curvilinear coordinates are equivalent to first order at zero separation for a circular orbit, $\left.\frac{\partial\, \delta \boldsymbol{x}_{\mathcal{R}}(t_k)}{\partial\, \delta \boldsymbol{x}_{\psi}(t_k)}\right|_{\delta \boldsymbol{x}_{\psi}(t_k)=\mathbf{0}} = \mathbf{I}_{6\times 6}$.

Using the linearization in Eq. (33), the time updated error covariance of the inertial Cartesian state can be written as

$$\begin{aligned} \mathbf{P}_{\mathcal{I},k|k-1} &= \mathrm{E}[\boldsymbol{X}_{\mathcal{I}}(t_k)\boldsymbol{X}_{\mathcal{I}}^T(t_k)] && (37)\\ &= \mathbf{J}_{\mathcal{I}\psi}(t_k)\mathbf{P}_{\psi,k|k-1}\mathbf{J}_{\mathcal{I}\psi}(t_k)^T && (38)\\ &= \mathbf{J}_{\mathcal{I}\psi}(t_k)\mathbf{\Phi}_{\psi,k}\mathbf{P}_{\psi,k-1|k-1}\mathbf{\Phi}_{\psi,k}^T\mathbf{J}_{\mathcal{I}\psi}(t_k)^T + \mathbf{J}_{\mathcal{I}\psi}(t_k)\mathbf{Q}_{\psi,k}\mathbf{J}_{\mathcal{I}\psi}(t_k)^T && (39)\\ &= \mathbf{\Phi}_{\mathcal{I},k}\mathbf{P}_{\mathcal{I},k-1|k-1}\mathbf{\Phi}_{\mathcal{I},k}^T + \mathbf{J}_{\mathcal{I}\psi}(t_k)\mathbf{Q}_{\psi,k}\mathbf{J}_{\mathcal{I}\psi}(t_k)^T && (40) \end{aligned}$$

Substituting Eq. (27) into Eq. (38) yields Eq. (39). Eqs. (39) and (40) are related through the chain rule and the linearization in Eq. (33) applied at time t_{k-1}. Comparing Eq. (40) and Eq. (7), it is clear that the process noise covariance of $\boldsymbol{x}_{\mathcal{I}}$ at time step k is

$$\mathbf{Q}_{\mathcal{I},k} = \mathbf{J}_{\mathcal{I}\psi}(t_k)\mathbf{Q}_{\psi,k}\mathbf{J}_{\mathcal{I}\psi}(t_k)^T \tag{41}$$

Since $\left.\frac{\partial\, \delta \boldsymbol{x}_{\mathcal{R}}(t_k)}{\partial\, \delta \boldsymbol{x}_{\psi}(t_k)}\right|_{\delta \boldsymbol{x}_{\psi}(t_k)=\mathbf{0}} = \mathbf{I}_{6\times 6}$, it is equivalent to compute the process noise covariance integral parameterized in the rectlinear coordinates $\delta\boldsymbol{x}_{\mathcal{R}}$, and then obtain $\mathbf{Q}_{\mathcal{I},k}$ through a linear mapping similar to Eq. (41). Thus a higher order mapping from $\mathbf{Q}_{\psi,k}$ to $\mathbf{Q}_{\mathcal{I},k}$ is required to glean the benefits of spherical coordinates over rectilinear coordinates.

Orbital Element State and Circular Orbit

This section describes a framework for modeling the process noise covariance of an absolute orbital element state by assuming a circular orbit. The set of equinoctial elements is considered as an example, but the developed approach can be applied to any orbital element state representation. The equinoctial elements are defined as

$$\boldsymbol{x}_{\mathcal{E}} = \begin{bmatrix} a \\ f \\ g \\ h \\ k \\ \lambda \end{bmatrix} = \begin{bmatrix} a \\ e\cos(\omega+\Omega) \\ e\sin(\omega+\Omega) \\ \tan(\frac{i}{2})\cos(\Omega) \\ \tan(\frac{i}{2})\sin(\Omega) \\ M+\omega+\Omega \end{bmatrix} \tag{42}$$

in terms of the classical Keplerian orbital elements a, e, i, Ω, w, and M. The state $\boldsymbol{x}_{\mathcal{E}}$ is singular for $i = 180^\circ$ and $e = 1$. Considering only two-body motion, the state transition matrix of $\boldsymbol{x}_{\mathcal{E}}$ is

$$\mathbf{\Phi}_{\mathcal{E}}(t,t_0) = \begin{bmatrix} 1 & \mathbf{0}_{1\times 4} & \mathbf{0} \\ \mathbf{0}_{4\times 1} & \mathbf{I}_{4\times 4} & \mathbf{0}_{4\times 1} \\ \frac{-3n}{2a}(t-t_0) & \mathbf{0}_{1\times 4} & 1 \end{bmatrix} \tag{43}$$

The time derivatives of the equinoctial elements are given by the Gauss Variational Equations, which can be written in matrix form as

$$\frac{d\boldsymbol{x}_{\mathcal{E}}}{dt} = \mathbf{G}(\boldsymbol{x}_{\mathcal{E}})\boldsymbol{d} + \begin{bmatrix} \mathbf{0}_{5\times 1} \\ n \end{bmatrix} \tag{44}$$

where $\boldsymbol{d} \in \mathbb{R}^3$ is the perturbing accelerations expressed in the RTN frame. Treating the process noise as unmodeled accelerations expressed in the RTN frame, $\mathbf{G}(\boldsymbol{x}_{\mathcal{E}}) \in \mathbb{R}^{6\times 3}$ is the process noise mapping matrix.

This matrix is[25]

$$\mathbf{\Gamma}_{\mathcal{E}} = \mathbf{G}(\boldsymbol{x}_{\mathcal{E}}) = \begin{bmatrix} \bar{A} & \bar{B} & 0 \\ \bar{C} & \bar{D} & \bar{E} \\ \bar{F} & \bar{G} & \bar{H} \\ 0 & 0 & \bar{I} \\ 0 & 0 & \bar{J} \\ \bar{K} & \bar{L} & \bar{M} \end{bmatrix} \tag{45}$$

where $\bar{A}, \bar{B}, \ldots, \bar{M}$ are each a scalar function of $\boldsymbol{x}_{\mathcal{E}}$, and their specific definitions are provided in Appendix A. The matrix $\mathbf{\Gamma}_{\mathcal{E}}$ contains trigonometric functions of the true longitude $l = \nu + \Omega + w$ where ν is the true anomaly. For a near-circular orbit, the approximations $f = g = 0$ and

$$l(t) = l(t_{k-1}) + \bar{n}_k(t - t_{k-1}) \tag{46}$$

can be made where

$$\bar{n}_k = \frac{1}{\Delta t_k} \int_{t_{k-1}}^{t_k} \dot{\theta}_s(t)\, dt = \frac{\Delta\theta_{s,k}}{\Delta t_k} \tag{47}$$

is the average spacecraft angular rate over the propagation interval $[t_{k-1}, t_k]$. These approximations become exact as the orbit eccentricity approaches zero. Here $\dot{\theta}_s$ is the time rate of change of the angle between the spacecraft position vector and an arbitrary fixed vector in the orbital plane. The variable $\Delta\theta_{s,k} = \theta_s(t_k) - \theta_s(t_{k-1})$ is the angle traversed by the spacecraft over the interval $[t_{k-1}, t_k]$. In the case of zero eccentricity, $\bar{n}_k$ is equal to the mean motion. For other orbital element state representations, any quickly varying orbital elements such as the true anomaly or argument of latitude can be approximated similar to Eq. (46).

The process noise covariance of the state $\boldsymbol{x}_{\mathcal{E}}$ at time step k, $\mathbf{Q}_{\mathcal{E},k}$, is computed by evaluating Eq. (24) and substituting into Eq. (23). Analytically evaluating Eq. (24) for each axis using Eq. (46) and assuming $f = g = 0$ yields

$$\mathbf{Q}^r_{\mathcal{E},k} = \widetilde{Q}_r \begin{pmatrix} p \\ \overline{\mu} \end{pmatrix} \begin{bmatrix} 0 & \ddots & \ddots & \ddots & \ddots & \ddots \\ 0 & \bar{\zeta}_{ss} & \ddots & \ddots & \ddots & \ddots \\ 0 & -\bar{\zeta}_{cs} & \bar{\zeta}_{cc} & \ddots & \ddots & \ddots \\ 0 & 0 & 0 & 0 & \ddots & \ddots \\ 0 & 0 & 0 & 0 & 0 & \ddots \\ 0 & -2\bar{\zeta}_s & 2\bar{\zeta}_c & 0 & 0 & 4\Delta t_k \end{bmatrix} \tag{48}$$

$$\mathbf{Q}^t_{\mathcal{E},k} = \widetilde{Q}_t(\mathbf{M}_t\mathbf{M}_t^T) \circ \begin{bmatrix} \Delta t_k & \ddots & \ddots & \ddots & \ddots & \ddots \\ \bar{\zeta}_c & \bar{\zeta}_{cc} & \ddots & \ddots & \ddots & \ddots \\ \bar{\zeta}_s & \bar{\zeta}_{cs} & \bar{\zeta}_{ss} & \ddots & \ddots & \ddots \\ 0 & 0 & 0 & 0 & \ddots & \ddots \\ 0 & 0 & 0 & 0 & 0 & \ddots \\ \frac{1}{2}\Delta t_k^2 & \bar{\zeta}_{tc} & \bar{\zeta}_{ts} & 0 & 0 & \frac{1}{3}\Delta t_k^3 \end{bmatrix} \tag{49}$$

$$\mathbf{Q}^n_{\mathcal{E},k} = \widetilde{Q}_n(\mathbf{M}_n\mathbf{M}_n^T) \circ \begin{bmatrix} 0 & \ddots & \ddots & \ddots & \ddots & \ddots \\ 0 & 0 & \ddots & \ddots & \ddots & \ddots \\ 0 & 0 & 0 & \ddots & \ddots & \ddots \\ 0 & 0 & 0 & \bar{\zeta}_{cc} & \ddots & \ddots \\ 0 & 0 & 0 & \bar{\zeta}_{cs} & \bar{\zeta}_{ss} & \ddots \\ 0 & 0 & 0 & k\bar{\zeta}_{cc} - h\bar{\zeta}_{cs} & k\bar{\zeta}_{cs} - h\bar{\zeta}_{ss} & k^2\bar{\zeta}_{cc} + h^2\bar{\zeta}_{ss} - 2kh\bar{\zeta}_{cs} \end{bmatrix} \tag{50}$$

with the auxilliary variables

$$\mathbf{M}_t = \begin{bmatrix} \frac{2a^2}{\hbar} & 2\sqrt{\frac{p}{\mu}} & 2\sqrt{\frac{p}{\mu}} & 0 & 0 & \frac{-3na}{\hbar} \end{bmatrix}^T \tag{51}$$

$$\mathbf{M}_n = \begin{bmatrix} 0 & 0 & 0 & \frac{1}{2}\sqrt{\frac{p}{\mu}}(1+h^2+k^2) & \frac{1}{2}\sqrt{\frac{p}{\mu}}(1+h^2+k^2) & \frac{-\hbar}{\mu} \end{bmatrix}^T \tag{52}$$

and

$$\begin{aligned}
\bar{\zeta}_c &= \int_{t_{k-1}}^{t_k} \cos\, l(\tau) d\tau = \frac{1}{\bar{n}_k}(\sin\, l_k - \sin\, l_{k-1}) \\
\bar{\zeta}_s &= \int_{t_{k-1}}^{t_k} \sin\, l(\tau) d\tau = -\frac{1}{\bar{n}_k}(\cos\, l_k - \cos\, l_{k-1}) \\
\bar{\zeta}_{cc} &= \int_{t_{k-1}}^{t_k} \cos^2\, l(\tau) d\tau = \frac{\Delta t_k}{2} + \frac{1}{4\bar{n}_k}(\sin\, 2l_k - \sin\, 2l_{k-1}) \\
\bar{\zeta}_{ss} &= \int_{t_{k-1}}^{t_k} \sin^2\, l(\tau) d\tau = \frac{\Delta t_k}{2} - \frac{1}{4\bar{n}_k}(\sin\, 2l_k - \sin\, 2l_{k-1}) \\
\bar{\zeta}_{cs} &= \int_{t_{k-1}}^{t_k} \cos\, l(\tau)\, \sin\, l(\tau) d\tau = -\frac{1}{4\bar{n}_k}(\cos\, 2l_k - \cos\, 2l_{k-1}) \\
\bar{\zeta}_{tc} &= \int_{t_{k-1}}^{t_k} (t_k - \tau)\cos\, l(\tau) d\tau = -\frac{1}{\bar{n}_k^2}(\bar{n}_k \Delta t_k \sin\, l_{k-1} + \cos\, l_k - \cos\, l_{k-1}) \\
\bar{\zeta}_{ts} &= \int_{t_{k-1}}^{t_k} (t_k - \tau)\sin\, l(\tau) d\tau = \frac{1}{\bar{n}_k^2}(\bar{n}_k \Delta t_k \cos\, l_{k-1} - \sin\, l_k + \sin\, l_{k-1})
\end{aligned} \tag{53}$$

Here $p = a(1-e^2)$ is the orbit semi-parameter, $\hbar = \sqrt{\mu p}$ is the magnitude of the angular momentum vector, and $l_k = l(t_k)$. Since the orbit is assumed circular, the semi-parameter can be replaced with the semi-major axis. Each matrix in Eqs. (48-50) is symmetric, so only the unique elements in the lower triangular portion of each matrix are specified. The symbol $\circ$ denotes the Hadamard product, which indicates element-wise multiplication of two matrices with the same dimensions.

Orbital Element State and Small Propagation Interval

Another approach to obtain a concise analytical solution to Eq. (5) for an orbital element state is to assume that the propagation interval $[t_{k-1}, t_k]$ is small such that any quickly varying orbital elements can be approximated as constant over that interval. Then all the equinoctial elements are constant when considering only two-body motion. In the case of the equinoctial elements, it is assumed that the true longitude is constant over the interval $[t_{k-1}, t_k]$. As a result, the process noise mapping matrix is constant over the interval $[t_{k-1}, t_k]$. For a constant $\mathbf{\Gamma}_{\mathcal{E}}$ and the state transition matrix in Eq. (43), the contributions to $\mathbf{Q}_{\mathcal{E},k}$ in each axis shown in Eq. (24) evaluate to

$$\begin{aligned}
\mathbf{Q}^r_{\mathcal{E},k} &= \widetilde{Q}_r \left(\Delta t_k \mathbf{\Gamma}_{\mathcal{E},r} \mathbf{\Gamma}^T_{\mathcal{E},r} + \frac{3n\Delta t_k^2}{4a} \begin{bmatrix} \mathbf{0}_{5\times 5} & \mathbf{S}_r \\ \mathbf{S}_r^T & \frac{n}{a}\bar{A}^2 \Delta t - 2\bar{A}\bar{K} \end{bmatrix} \right) \\
\mathbf{Q}^t_{\mathcal{E},k} &= \widetilde{Q}_t \left(\Delta t_k \mathbf{\Gamma}_{\mathcal{E},t} \mathbf{\Gamma}^T_{\mathcal{E},t} + \frac{3n\Delta t_k^2}{4a} \begin{bmatrix} \mathbf{0}_{5\times 5} & \mathbf{S}_t \\ \mathbf{S}_t^T & \frac{n}{a}\bar{B}^2 \Delta t - 2\bar{B}\bar{L} \end{bmatrix} \right) \\
\mathbf{Q}^n_{\mathcal{E},k} &= \widetilde{Q}_n \Delta t_k \mathbf{\Gamma}_{\mathcal{E},n} \mathbf{\Gamma}^T_{\mathcal{E},n}
\end{aligned} \tag{54}$$

where $\mathbf{S}_r = -[\bar{A}^2 \;\; \bar{A}\bar{C} \;\; \bar{A}\bar{F} \;\; 0 \;\; 0]^T$ and $\mathbf{S}_t = -[\bar{B}^2 \;\; \bar{B}\bar{D} \;\; \bar{B}\bar{G} \;\; 0 \;\; 0]^T$. The first, second, and third columns of $\mathbf{\Gamma}_{\mathcal{E}}$ are denoted $\mathbf{\Gamma}_{\mathcal{E},r}$, $\mathbf{\Gamma}_{\mathcal{E},t}$, and $\mathbf{\Gamma}_{\mathcal{E},n}$ respectively. Eq. (54) is evaluated using the true longitude halfway through the propagation interval $[t_{k-1}, t_k]$ at time $\frac{t_{k-1}+t_k}{2}$.

Both of the developed equinoctial element process noise covariance models provide important insights. For example, notice from Eqs. (44-45) that the time evolution of the equinoctial elements h and k are only

affected by perturbing accelerations in the normal direction. As a result, only unmodeled accelerations in the normal direction contribute to the process noise covariance of h and k as is shown in the model described by Eqs. (48-53) and the model in Eq. (54). In both of these models, the process noise covariance of h is small when the true longitude is near $l = \frac{(2n-1)\pi}{2}$ throughout the interval $[t_{k-1}, t_k]$ for any integer n. This occurs because perturbing accelerations have no effect on h at $l = \frac{(2n-1)\pi}{2}$ since $\bar{I}$ in Eq. (45) is zero. Similarly, the process noise covariance of k is small when the true longitude is near $l = n\pi$ throughout the interval $[t_{k-1}, t_k]$.

RELATIVE PROCESS NOISE COVARIANCE FOR SMALL SEPARATIONS

If the interspacecraft separation is small compared to the orbit radius, then the nonlinear dynamical model of the relative state $\delta\boldsymbol{x}_\alpha$ can be linearized about zero interspacecraft separation over the propagation interval $[t_{k-1}, t_k]$, resulting in a linear time-varying system

$$\delta\dot{\boldsymbol{x}}_\alpha(t) = \mathbf{A}_{\delta\alpha}(t)\delta\boldsymbol{x}_\alpha(t) + \mathbf{B}_{\delta\alpha}(t)\delta\boldsymbol{u}(t) + \mathbf{\Gamma}_{\delta\alpha}(t)\delta\boldsymbol{\epsilon}(t) \tag{55}$$

The plant matrix, control input matrix, and process noise mapping matrix of the relative state are

$$\mathbf{A}_{\delta\alpha}(t) = \frac{\partial\delta\dot{\boldsymbol{x}}_\alpha(t)}{\partial\delta\boldsymbol{x}_\alpha(t)}, \qquad \mathbf{B}_{\delta\alpha}(t) = \frac{\partial\delta\dot{\boldsymbol{x}}_\alpha(t)}{\partial\delta\boldsymbol{u}(t)}, \qquad \mathbf{\Gamma}_{\delta\alpha}(t) = \frac{\partial\delta\dot{\boldsymbol{x}}_\alpha(t)}{\partial\delta\boldsymbol{\epsilon}(t)} \tag{56}$$

evaluated at zero interspacecraft separation. The subscript δ indicates a matrix corresponds to a relative state, and the particular relative state is specified by the subscript α. The differential control inputs $\delta\boldsymbol{u} = \boldsymbol{u}_d - \boldsymbol{u}_c$ are the difference between the control inputs of the deputy and chief expressed in the chief RTN frame. Similarly, the differential unmodeled accelerations $\delta\boldsymbol{\epsilon} = \boldsymbol{\epsilon}_d - \boldsymbol{\epsilon}_c$ are the difference between the deputy and chief unmodeled accelerations expressed in the chief RTN frame with autocovariance

$$\begin{aligned}
\mathrm{E}[\delta\boldsymbol{\epsilon}(t)\delta\boldsymbol{\epsilon}(\tau)^T] &= \mathrm{E}[\boldsymbol{\epsilon}_d(t)\boldsymbol{\epsilon}_d(\tau)^T] + \mathrm{E}[\boldsymbol{\epsilon}_c(t)\boldsymbol{\epsilon}_c(\tau)^T] - \mathrm{E}[\boldsymbol{\epsilon}_d(t)\boldsymbol{\epsilon}_c(\tau)^T] - \mathrm{E}[\boldsymbol{\epsilon}_c(t)\boldsymbol{\epsilon}_d(\tau)^T] \\
&= (\widetilde{\mathbf{Q}}_d + \widetilde{\mathbf{Q}}_c - \widetilde{\mathbf{Q}}_{dc} - \widetilde{\mathbf{Q}}_{cd})\delta(t-\tau) \\
&= \widetilde{\mathbf{Q}}_\delta\delta(t-\tau)
\end{aligned} \tag{57}$$

Here $\widetilde{\mathbf{Q}}_\delta = (\widetilde{\mathbf{Q}}_d + \widetilde{\mathbf{Q}}_c - \widetilde{\mathbf{Q}}_{dc} - \widetilde{\mathbf{Q}}_{cd}) \in \mathbb{R}^{3\times3}$ is the power spectral density of $\delta\boldsymbol{\epsilon}$. The power spectral densities of the chief and deputy unmodeled accelerations are $\widetilde{\mathbf{Q}}_c$ and $\widetilde{\mathbf{Q}}_d$ respectively. The cross power spectral density is $\mathrm{E}[\boldsymbol{\epsilon}_d(t)\boldsymbol{\epsilon}_c(\tau)^T] = \widetilde{\mathbf{Q}}_{dc} = \widetilde{\mathbf{Q}}_{cd}^T$. Following a similar derivation to that of Eqs. (5 - 7), the propagated error covariance of $\delta\boldsymbol{x}_\alpha$ for the linearized system in Eq. (55) is

$$\mathbf{P}_{\delta\alpha,k|k-1} = \mathrm{E}[(\delta\boldsymbol{x}_\alpha(t_k) - \delta\hat{\boldsymbol{x}}_{\alpha,k|k-1})(\delta\boldsymbol{x}_\alpha(t_k) - \delta\hat{\boldsymbol{x}}_{\alpha,k|k-1})^T] \tag{58}$$

$$= \mathbf{\Phi}_{\delta\alpha,k}\mathbf{P}_{\delta\alpha,k-1|k-1}\mathbf{\Phi}_{\delta\alpha,k}^T + \mathbf{Q}_{\delta\alpha,k} \tag{59}$$

where the process noise covariance of $\delta\boldsymbol{x}_\alpha$ at time step k is

$$\mathbf{Q}_{\delta\alpha,k} = \int_{t_{k-1}}^{t_k} \mathbf{\Phi}_{\delta\alpha}(t_k,\tau)\mathbf{\Gamma}_{\delta\alpha}(\tau)\widetilde{\mathbf{Q}}_\delta\mathbf{\Gamma}_{\delta\alpha}(\tau)^T\mathbf{\Phi}_{\delta\alpha}(t_k,\tau)^T d\tau \tag{60}$$

The state transition matrix $\mathbf{\Phi}_{\delta\alpha,k} = \mathbf{\Phi}_{\delta\alpha}(t_k, t_{k-1})$ propagates the relative state $\delta\boldsymbol{x}_\alpha$ from time t_{k-1} to time t_k. Due to the structure of Eq. (60), $\mathbf{Q}_{\delta\alpha,k}$ is guaranteed symmetric and positive semi-definite when $\widetilde{\mathbf{Q}}_\delta$ is symmetric and positive semi-definite . Throughout this paper, $\widetilde{\mathbf{Q}}_\delta$ is expressed in the chief RTN frame, denoted $\widetilde{\mathbf{Q}}_\delta^{\mathcal{R}}$. For simplicity, it is assumed that $\widetilde{\mathbf{Q}}_\delta^{\mathcal{R}}$ is diagonal where

$$\widetilde{\mathbf{Q}}_\delta^{\mathcal{R}} = \begin{bmatrix} \widetilde{Q}_{\delta r} & 0 & 0 \\ 0 & \widetilde{Q}_{\delta t} & 0 \\ 0 & 0 & \widetilde{Q}_{\delta n} \end{bmatrix} \tag{61}$$

Relative Cartesian State

This section derives a model of the process noise covariance for the relative state $\delta\boldsymbol{x}_{\mathcal{R}}$. First, consider the relative curvilinear state $\delta\boldsymbol{x}_{\psi}$ defined in Eq. (20) with differential unmodeled accelerations expressed in the chief RTN frame. It is deduced from Eqs. (17-19) that the corresponding process noise mapping matrix $\boldsymbol{\Gamma}_{\delta\psi}$ matches that shown in Eq. (28). Assuming a circular chief orbit and two-body motion, the state transition matrix of $\delta\boldsymbol{x}_{\psi}$ is given in Eq. (21). Thus, the process noise covariance of $\delta\boldsymbol{x}_{\psi}$ at time step k, denoted $\mathbf{Q}_{\delta\psi,k}$, is obtained by substituting Eq. (21), Eq. (28), and Eq. (61) into Eq. (60) and analytically evaluating the integral. Since the state transition matrix and process noise mapping matrix match those used to compute $\mathbf{Q}_{\psi,k}$ through Eq. (5), then $\mathbf{Q}_{\delta\psi,k}$ is given by Eqs. (23 - 32) after making the substitutions $\mathbf{Q}_{\psi,k} = \mathbf{Q}_{\delta\psi,k}$ and $\widetilde{\mathbf{Q}}^{\mathcal{R}} = \widetilde{\mathbf{Q}}^{\mathcal{R}}_{\delta}$. The process noise covariance of $\delta\boldsymbol{x}_{\mathcal{R}}$, denoted $\mathbf{Q}_{\delta\mathcal{R},k}$, can then be computed through a linear mapping of $\mathbf{Q}_{\delta\psi,k}$. The linear mapping results in $\mathbf{Q}_{\delta\mathcal{R},k} = \mathbf{Q}_{\delta\psi,k}$ since $\frac{\partial\, \delta\boldsymbol{x}_{\mathcal{R}}(t_k)}{\partial\, \delta\boldsymbol{x}_{\psi}(t_k)}\big|_{\delta\boldsymbol{x}_{\psi}(t_k)=\mathbf{0}} = \mathbf{I}_{6\times 6}$. Just as in the absolute Cartesian state case, a higher order uncertainty mapping is required to benefit from computing the process noise covariance integral parameterized in spherical coordinates instead of the rectlinear coordinates $\delta\boldsymbol{x}_{\mathcal{R}}$.

Relative Orbital Element State

A framework for modeling the process noise covariance of a relative orbital element state is demonstrated using the set of relative orbital elements[15]

$$\delta\boldsymbol{x}_{\mathcal{E}} = \begin{bmatrix} (a_d - a_c)/a_c \\ \lambda_d - \lambda_c \\ f_d - f_c \\ g_d - g_c \\ h_d - h_c \\ k_d - k_c \end{bmatrix} \tag{62}$$

as an example. However, this approach can be applied to any set of relative orbital elements. The relative state in Eq. (62) is a function of the equinoctial orbital elements of the chief and deputy, which are defined in Eq. (42). Consider a similar set of relative orbital elements

$$\delta\boldsymbol{x}_{\mathcal{E}'} = \boldsymbol{x}^d_{\mathcal{E}} - \boldsymbol{x}^c_{\mathcal{E}} \tag{63}$$

where $\boldsymbol{x}^c_{\mathcal{E}}$ and $\boldsymbol{x}^d_{\mathcal{E}}$ are the equinoctial elements of the chief and deputy respectively. Linearizing the system about zero interspacecraft separation and considering only two-body motion, the state transition matrix of $\delta\boldsymbol{x}_{\mathcal{E}'}$ matches that shown in Eq. (43). Since the system is linearized about zero interspacecraft separation, the semi-major axis and mean motion in the state transition matrix can refer to the chief or deputy. For consistency, the chief parameters will be used throughout this section whenever there is an arbitrary choice between the parameters of the chief and deputy.

The time derivative of $\delta\boldsymbol{x}_{\mathcal{E}'}$ can be expanded using the chain rule as

$$\frac{d\delta\boldsymbol{x}_{\mathcal{E}'}}{dt} = \frac{\partial\delta\boldsymbol{x}_{\mathcal{E}'}}{\partial\boldsymbol{x}^d_{\mathcal{E}}}\frac{d\boldsymbol{x}^d_{\mathcal{E}}}{dt} + \frac{\partial\delta\boldsymbol{x}_{\mathcal{E}'}}{\partial\boldsymbol{x}^c_{\mathcal{E}}}\frac{d\boldsymbol{x}^c_{\mathcal{E}}}{dt} \tag{64}$$

The partial derivatives of $\delta\boldsymbol{x}_{\mathcal{E}'}$ with respect to $\boldsymbol{x}^d_{\mathcal{E}}$ and $\boldsymbol{x}^c_{\mathcal{E}}$ are

$$\frac{\partial\delta\boldsymbol{x}_{\mathcal{E}'}}{\partial\boldsymbol{x}^d_{\mathcal{E}}} = \mathbf{I}_{6\times 6}, \qquad \frac{\partial\delta\boldsymbol{x}_{\mathcal{E}'}}{\partial\boldsymbol{x}^c_{\mathcal{E}}} = -\mathbf{I}_{6\times 6} \tag{65}$$

Substituting Eqs. (44) and (65) into Eq. (64) and assuming zero interspacecraft separation yields

$$\frac{d\delta\boldsymbol{x}_{\mathcal{E}'}}{dt} = \mathbf{G}(\boldsymbol{x}^d_{\mathcal{E}})\underset{c\to d}{\mathbf{R}}\boldsymbol{d}_d - \mathbf{G}(\boldsymbol{x}^c_{\mathcal{E}})\boldsymbol{d}_c \tag{66}$$

$$= \mathbf{G}(\boldsymbol{x}^c_{\mathcal{E}})\delta\boldsymbol{d} \tag{67}$$

where $\delta \boldsymbol{d} = \boldsymbol{d}_d - \boldsymbol{d}_c$ is the difference between the deputy and chief perturbing accelerations expressed in the chief RTN frame. The matrix $\underset{c \to d}{\mathbf{R}} \in \mathbb{R}^{3\times3}$ rotates vectors from the chief RTN frame to the deputy RTN frame and is the identity matrix for zero interspacecraft separation. Thus the process noise mapping matrix is $\boldsymbol{\Gamma}_{\delta\mathcal{E}'} = \mathbf{G}(\boldsymbol{x}^c_{\mathcal{E}})$, which matches that of the absolute equinoctial orbital elements as shown in Eq. (45).

Since the state transition matrix and process noise mapping matrix of $\delta\boldsymbol{x}_{\mathcal{E}'}$ match that of the absolute equinoctial elements, the expressions for $\mathbf{Q}_{\delta\mathcal{E}',k}$ and $\mathbf{Q}_{\mathcal{E},k}$ are equivalent except that the expression for $\mathbf{Q}_{\delta\mathcal{E}',k}$ considers differential unmodeled accelerations. Thus, $\mathbf{Q}_{\delta\mathcal{E}',k}$ can be computed through Eq. (23) and either Eqs. (48-53) for a near-circular chief or through Eqs. (54) for a small propagation interval by making the substitutions $\mathbf{Q}_{\mathcal{E},k} = \mathbf{Q}_{\delta\mathcal{E}',k}$ and $\widetilde{\mathbf{Q}}^{\mathcal{R}} = \widetilde{\mathbf{Q}}^{\mathcal{R}}_{\delta}$ where $\widetilde{\mathbf{Q}}^{\mathcal{R}}_{\delta}$ is defined in Eq. (61). Then following the approach in Eqs. (37-41), the process noise covariance of $\delta\boldsymbol{x}_{\mathcal{E}}$ is

$$\mathbf{Q}_{\delta\mathcal{E},k} = \mathbf{J}_{\delta\mathcal{E}}(t_k)\mathbf{Q}_{\delta\mathcal{E}',k}\mathbf{J}_{\delta\mathcal{E}}(t_k)^T \tag{68}$$

where

$$\mathbf{J}_{\delta\mathcal{E}}(t_k) = \left.\frac{\partial\delta\boldsymbol{x}_{\mathcal{E}}}{\partial\delta\boldsymbol{x}_{\mathcal{E}'}}\right|_{\delta\boldsymbol{x}_{\mathcal{E}'}=\mathbf{0}} = \begin{bmatrix} \frac{1}{a_c} & \mathbf{0}_{1\times4} & 0 \\ 0 & \mathbf{0}_{1\times4} & 1 \\ \mathbf{0}_{4\times1} & \mathbf{I}_{4\times4} & \mathbf{0}_{4\times1} \end{bmatrix} \tag{69}$$

RELATIVE PROCESS NOISE COVARIANCE FOR LARGE SEPARATIONS

If the interspacecraft separation is large, the linearization about zero interspacecraft separation utilized in the previous section may introduce significant errors. Instead of assuming small separations, this section constructs the process noise covariance of a relative spacecraft state by assuming that the interspacecraft separation is large enough that the unmodeled accelerations of the chief are uncorrelated with those of the deputy. In general,

$$\delta\boldsymbol{x}_\alpha(t_k) = \boldsymbol{f}(\boldsymbol{x}^d_\beta(t_k), \boldsymbol{x}^c_\beta(t_k)) \tag{70}$$

where $\boldsymbol{f}(\cdot)$ is some function. The absolute states of the deputy and chief are $\boldsymbol{x}^d_\beta$ and $\boldsymbol{x}^c_\beta$ respectively where β denotes the specific absolute state representation. Eq. (70) can be approximated through a first-order Taylor series expansion as

$$\delta\boldsymbol{x}_\alpha(t_k) = \delta\hat{\boldsymbol{x}}_{\alpha,k|k-1} + \mathbf{J}_d(t_k)(\boldsymbol{x}^d_\beta(t_k) - \hat{\boldsymbol{x}}^d_{\beta,k|k-1}) + \mathbf{J}_c(t_k)(\boldsymbol{x}^c_\beta(t_k) - \hat{\boldsymbol{x}}^c_{\beta,k|k-1}) \tag{71}$$

which is valid for small deviations of the estimated chief and deputy absolute states from their corresponding true states. Here the partial derivatives

$$\mathbf{J}_d(t_k) = \frac{\partial\delta\boldsymbol{x}_\alpha(t_k)}{\partial\boldsymbol{x}^d_\beta(t_k)}, \qquad \mathbf{J}_c(t_k) = \frac{\partial\delta\boldsymbol{x}_\alpha(t_k)}{\partial\boldsymbol{x}^c_\beta(t_k)} \tag{72}$$

are evaluated at the mean state estimate. If the interspacecraft separation is large, it can reasonably be assumed that the chief unmodeled accelerations are uncorrelated with those of the deputy . Using this assumption and the linearization in Eq. (71), the propagated error covariance of $\delta\boldsymbol{x}_\alpha$ can be written as

$$\mathbf{P}_{\delta\alpha,k|k-1} = \mathrm{E}[(\delta\boldsymbol{x}_\alpha(t_k) - \delta\hat{\boldsymbol{x}}_{\alpha,k|k-1})(\delta\boldsymbol{x}_\alpha(t_k) - \delta\hat{\boldsymbol{x}}_{\alpha,k|k-1})^T] \tag{73}$$

$$= \boldsymbol{\Phi}_{\delta\alpha,k}\mathbf{P}_{\delta\alpha,k-1|k-1}\boldsymbol{\Phi}^T_{\delta\alpha,k} + \mathbf{J}_d(t_k)\mathbf{Q}^d_{\alpha,k}\mathbf{J}_d(t_k)^T + \mathbf{J}_c(t_k)\mathbf{Q}^c_{\alpha,k}\mathbf{J}_c(t_k)^T \tag{74}$$

after some manipulation. Here $\mathbf{Q}^d_{\beta,k}$ and $\mathbf{Q}^c_{\beta,k}$ are the process noise covariances of the absolute chief and deputy states respectively at time step k. Comparing Eqs. (59) and (74), it is clear that the process noise covariance of $\delta\boldsymbol{x}_\alpha$ at time step k is

$$\mathbf{Q}_{\delta\alpha,k} = \mathbf{J}_d(t_k)\mathbf{Q}^d_{\beta,k}\mathbf{J}_d(t_k)^T + \mathbf{J}_c(t_k)\mathbf{Q}^c_{\beta,k}\mathbf{J}_c(t_k)^T \tag{75}$$

The matrices $\mathbf{Q}^d_{\beta,k}$ and $\mathbf{Q}^c_{\beta,k}$ can be computed using any process noise covariance models for absolute spacecraft states including those developed in the previous sections. Eq. (75) guarantees $\mathbf{Q}_{\delta\alpha,k}$ is positive semi-definite provided that $\mathbf{Q}^d_{\beta,k}$ and $\mathbf{Q}^c_{\beta,k}$ are positive semi-definite.

As an example, consider the relative Cartesian state $\delta\boldsymbol{x}_{\mathcal{R}}$ defined in Eq. (12), which is a function of the absolute, inertial Cartesian states of the chief and deputy denoted $\boldsymbol{x}_{\mathcal{I}}^{c}$ and $\boldsymbol{x}_{\mathcal{I}}^{d}$ respectively. The process noise covariance of $\delta\boldsymbol{x}_{\mathcal{R}}$ can be modeled through Eq. (75) where the process noise covariances of the chief and deputy inertial Cartesian states, $\mathbf{Q}_{\mathcal{I},k}^{c}$ and $\mathbf{Q}_{\mathcal{I},k}^{d}$, are separately computed using the model shown in Eqs. (23) and (29-32). The required partial derivatives in Eq. (75) are

$$\mathbf{J}_d(t_k) = \frac{\partial \delta\boldsymbol{x}_{\mathcal{R}}(t_k)}{\partial \boldsymbol{x}_{\mathcal{I}}^{d}(t_k)} = \begin{bmatrix} \underset{\mathcal{I}\rightarrow\mathcal{R}}{\mathbf{R}}(t_k) & \mathbf{0}_{3\times 3} \\ -\boldsymbol{w}^{\times}\underset{\mathcal{I}\rightarrow\mathcal{R}}{\mathbf{R}}(t_k) & \underset{\mathcal{I}\rightarrow\mathcal{R}}{\mathbf{R}}(t_k) \end{bmatrix} \tag{76}$$

The partial derivatives $\mathbf{J}_c(t_k) = \frac{\partial \delta\boldsymbol{x}_{\mathcal{R}}(t_k)}{\partial \boldsymbol{x}_{\mathcal{I}}^{c}(t_k)}$ can be approximated through finite differencing but should be derived analytically in the future.

As another example, the process noise covariance of the relative orbital element state $\delta\boldsymbol{x}_{\mathcal{E}}$ defined in Eq. (62) can be modeled by Eq. (75) where $\mathbf{Q}_{\mathcal{E},k}^{c}$ and $\mathbf{Q}_{\mathcal{E},k}^{d}$ are each computed through Eqs. (23) and (48-53) for a near-circular orbit or through Eqs. (23) and (54) for a small propagation interval. In this case, the required partial derivatives of the relative state with respect to the absolute states of the deputy and chief are

$$\mathbf{J}_d(t_k) = \frac{\partial \delta\boldsymbol{x}_{\mathcal{E}}(t_k)}{\partial \boldsymbol{x}_{\mathcal{E}}^{d}(t_k)} = \begin{bmatrix} \frac{1}{a_c} & \mathbf{0}_{1\times 4} & 0 \\ 0 & \mathbf{0}_{1\times 4} & 1 \\ \mathbf{0}_{4\times 1} & \mathbf{I}_{4\times 4} & \mathbf{0}_{4\times 1} \end{bmatrix} \tag{77}$$

$$\mathbf{J}_c(t_k) = \frac{\partial \delta\boldsymbol{x}_{\mathcal{E}}(t_k)}{\partial \boldsymbol{x}_{\mathcal{E}}^{c}(t_k)} = \begin{bmatrix} \frac{-a_d}{a_c^2} & \mathbf{0}_{1\times 4} & 0 \\ 0 & \mathbf{0}_{1\times 4} & -1 \\ \mathbf{0}_{4\times 1} & -\mathbf{I}_{4\times 4} & \mathbf{0}_{4\times 1} \end{bmatrix} \tag{78}$$

evaluated at the mean state estimate.

NUMERICAL VALIDATION

This section validates the developed analytical process noise covariance models by comparing them to numerical solutions of the integrals they approximate. The numerical solutions are considered the reference truth and assume unperturbed Keplerian motion about a central body. Two error metrics are employed. The first error metric is

$$\Delta t_{min} = \min\{\Delta t \ : \ |(Q_{ii}(\Delta t)^{\frac{1}{2}} - \hat{Q}_{ii}(\Delta t)^{\frac{1}{2}})/Q_{ii}(\Delta t)^{\frac{1}{2}}| \geq 0.15 \ \text{ for any } 1 \leq i \leq 6\} \tag{79}$$

which is the smallest propagation interval length for which the fractional error in any modeled process noise standard deviation is greater than or equal to 0.15. The element in the i^{th} row and column of the process noise covariance as determined numerically and analytically are Q_{ii} and $\hat{Q}_{ii}$ respectively. The second error metric is the maximum fractional error in any one element of the modeled process noise standard deviation for any propagation interval length up to one orbit. This error metric is defined as

$$\delta_{max} = \max\{|(Q_{ii}(\Delta t)^{\frac{1}{2}} - \hat{Q}_{ii}(\Delta t)^{\frac{1}{2}})/Q_{ii}(\Delta t)^{\frac{1}{2}}| \ : 1 \leq i \leq 6, \ 0 \leq \Delta t \leq 1 \text{ orbit}\} \tag{80}$$

Note that all the presented results are valid for any orbit semi-major axis because the associated time intervals are normalized by the orbit period.

Absolute Process Noise Covariance

The analytical process noise covariance models of the absolute Cartesian state $\boldsymbol{x}_{\mathcal{I}}$ and equinoctial orbital element state $\boldsymbol{x}_{\mathcal{E}}$ are each compared against the corresponding numerical solution of Eq. (5) obtained through fourth-order Runge-Kutta numerical integration assuming unperturbed Keplerian motion. While eccentricity is varied, the orbit inclination and right ascension of the ascending node are each 45°. The initial mean longitude is 90°. The spacecraft trajectory nominally starts at periapsis, although periapsis is not well defined for small eccentricities, in order to maximize the effects of eccentricity. The absolute power spectral density

is as shown in Eq. (22). In one scenario, $\widetilde{Q}_r$, $\widetilde{Q}_t$, and $\widetilde{Q}_n$ are all equal to a single value denoted $\widetilde{Q}^*$. In a second scenario, $\widetilde{Q}_r = \widetilde{Q}_n = \widetilde{Q}^*$ and $\widetilde{Q}_t = 10\widetilde{Q}^*$, which is representative of a case where atmospheric drag is the largest source of unmodeled accelerations. Notice in Eq. (5) that each element of the process noise covariance is a linear function of the elements of the power spectral density. Since the nonzero elements of the power spectral density are each a linear function of $\widetilde{Q}^*$, each process noise standard deviation is some scalar times $(\widetilde{Q}^*)^{\frac{1}{2}}$ for both the numerical and considered analytical solutions. Thus the fractional error of each process noise standard deviation is the same regardless of the simulated value of $\widetilde{Q}^*$.

The new model for equinoctial elements in Eq. (54) and the widely used model for an inertial Cartesian state in Eq. (11) both assume a small propagation interval Δt_k. To determine the range of propagation interval lengths for which these models can be accurately applied, Δt_{min} is plotted in Figure 2 as a function of eccentricity. The spacecraft angular velocity is greatest at periapsis and increases with increasing eccentricity, more quickly breaking the assumptions of these models. Thus, Δt_{min} tends to decrease for larger eccentricities in Figure 2 for both models, and both models generally perform better when the propagation interval is not near periapsis. The equinoctial element model outperforms the Cartesian model. Interestingly, Δt_{min} for the Cartesian model decreases significantly when the noise is predominantly in the transverse axis.

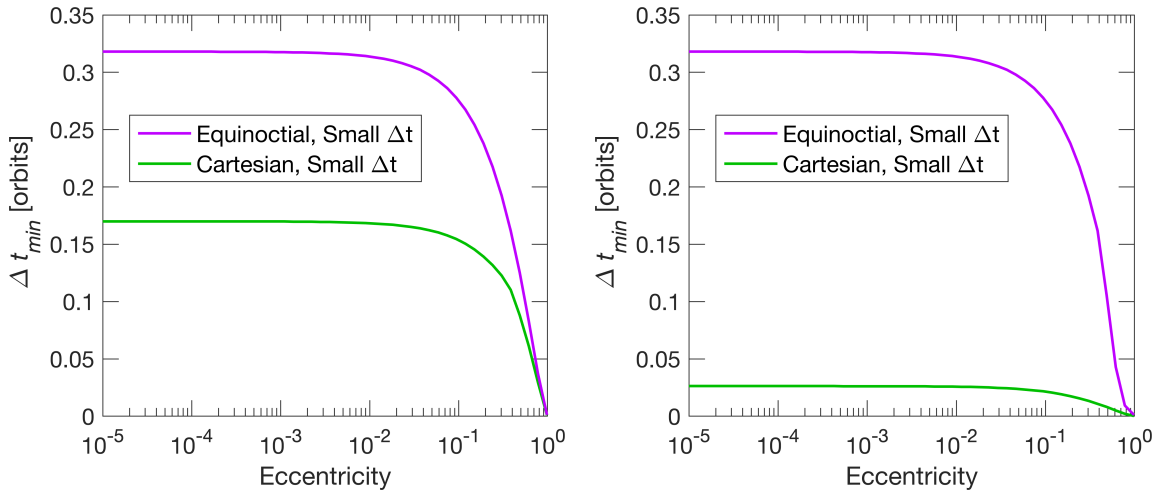

(a) Equal Noise in Each RTN Axis

(b) Transverse Dominant Noise

Figure 2: Comparison of Δt_{min} for the new process noise covariance model in Eq. (54) for equinoctial elements and the widely used model in Eq. (11) for an inertial Cartesian state.

The analytical models for equinoctial elements and Cartesian coordinates shown in Eq. (41) and Eqs. (48-53) respectively assume a circular orbit. In order to quantify the maximum orbit eccentricity for which these models can be applied, δ_{max} is plotted in Figure 3 as a function of eccentricity for the case of equal noise in each axis. The results of the transverse dominant noise case were nearly identical. The equinoctial model is valid for larger eccentricities than the Cartesian model. For example, δ_{max} is less than 0.1 for eccentricities less than about 0.09 and 0.02 for the equinoctial and Cartesian models respectively. Since δ_{max} is the largest fractional error over a full orbit, the fractional errors are smaller on average. Depending on the particular application, $\delta_{max} \leq 0.1$ may provide sufficient accuracy. The developed model for equinoctial elements in Eq. (54) and the widely used model for an inertial Cartesian state in Eq. (11) are also included in Figure 3 for reference. Since both of these models assume small propagation intervals and δ_{max} considers intervals up to an entire orbit, it is not surprising that $\delta_{max} > 1$ for these models.

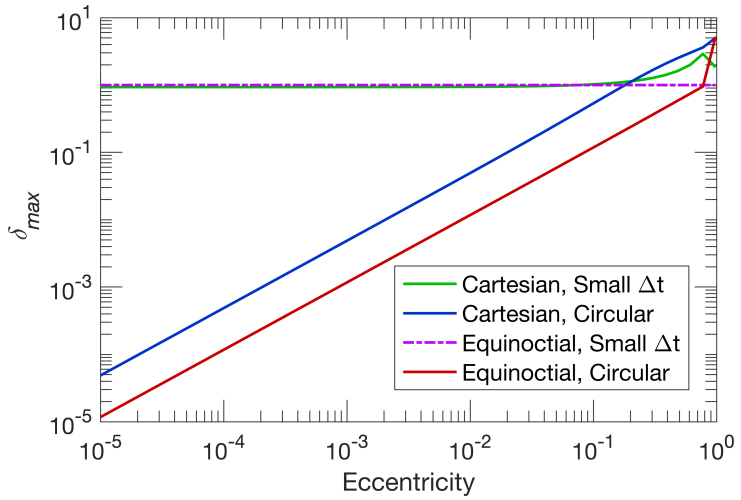

Figure 3: Comparison of δ_{max} for the process noise covariance models in Eq. (41) and Eq. (54) that assume a small propagation interval and the models in Eq. (41) and Eqs. (48-53) that assume a circular orbit.

Relative Process Noise Covariance

Consider two spacecraft where the chief has an eccentricity of 1×10^{-3} and an inclination and right ascension of the ascending node of $45°$. The initial chief equinoctial elements are $[f, g, h, k, \lambda] = [0, 1 \times 10^{-3}, 0.2929, 0.2929, 135°]$. The deputy equinoctial elements all match those of the chief with the exception of the initial mean longitude, which is varied. As a result, the two spacecraft are primarily separated in the along-track direction as described by the relative mean longitude, $\delta\lambda$. For simplicity, the unmodeled accelerations of the deputy are considered to be uncorrelated with those of the chief. Consequently, the reference truth process noise covariance of the relative states $\delta\boldsymbol{x}_{\mathcal{R}}$ and $\delta\boldsymbol{x}_{\mathcal{E}}$ are computed through Eq. (75). The reference truth process noise covariances of the chief and deputy employed in Eq. (75) are obtained through fourth-order Runge-Kutta numerical integration of Eq. (5) considering unperturbed Keplerian motion. The unmodeled acceleration power spectral density for each spacecraft is as shown in Eq. (22) where each diagonal element is equal to $\widetilde{Q}^*$ for both spacecraft. The presented results hold for any $\widetilde{Q}^*$.

Two approaches were taken to develop process noise covariance models for relative spacecraft states by assuming either small or large interspacecraft separation. Both approaches can utilize any absolute process noise covariance model. However, here the absolute model in Eq. (41) used when constructing the process noise covariance of $\delta\boldsymbol{x}_{\mathcal{R}}$, and the absolute model in Eqs. (48-53) is used when constructing the process noise covariance of $\delta\boldsymbol{x}_{\mathcal{E}}$. Since the employed absolute models assume circular orbits, the modeled relative process noise covariance incurs errors due to eccentricity whether the small or large separation approach is applied. The small separation framework additionally incurs errors due to interspacecraft separation. In order to quantify these errors, δ_{max} is plotted in Figure 4 for the considered analytical models. As expected, δ_{max} for each large separation model is similar to δ_{max} for the corresponding absolute model for an eccentricity of 1×10^{-3} (See Figure 3). For small separations, δ_{max} is similar for each large separation model and the corresponding small separation model. However, δ_{max} grows for the small separation models as the interspacecraft separation increases. Overall, the equinoctial element models outperform the Cartesian models. For example, $\delta_{max} \leq 0.1$ for the Cartesian and equinoctial small separation models for $\delta\lambda \leq 2 \times 10^{-3}$ and $\delta\lambda \leq 0.1$ respectively. These angles can be approximately transformed to interspacecraft distances through multiplication with the orbit semi-major axis. For example, for a semi-major axis of $10,000$ km, $\delta\lambda = 2 \times 10^{-3}$ corresponds to 20 km, and $\delta\lambda = 0.1$ corresponds to 1,000 km.

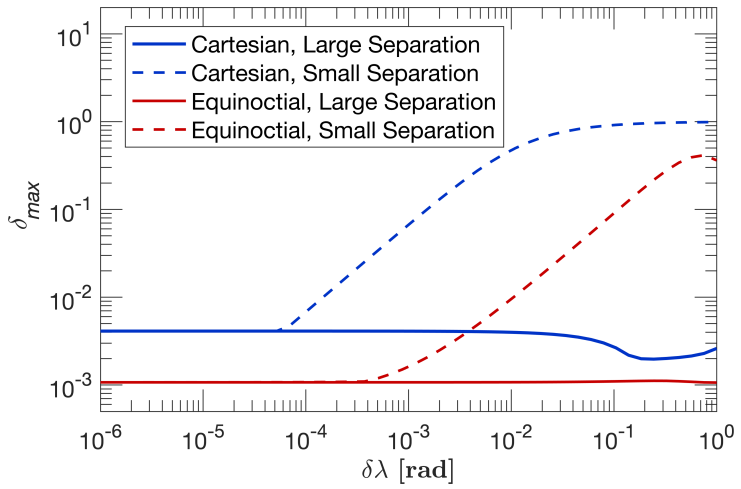

Figure 4: Comparison of δ_{max} for the developed relative process noise covariance models, which assume either small or large interspacecraft separation.

CONCLUSIONS

Accurate process noise modeling is essential for optimal orbit determination in a discrete-time Kalman filtering framework as well as for satellite conjunction analysis. A common approach to process noise modeling called state noise compensation (SNC) treats the process noise as zero-mean Gaussian white noise unmodeled accelerations. The resulting process noise covariance can be evaluated numerically. However, analytical solutions are desirable because they are computationally efficient and provide insight into system behavior. An analytical SNC model that assumes kinematic spaceraft motion with zero nominal acceleration is widely used, but this model is restricted to an absolute Cartesian state and small propagation intervals. Furthermore, analytical SNC models for absolute orbital element states and relative spacecraft states are not currently available. This paper first develops a new analytical SNC process noise covariance model for an inertial Cartesian spacecraft state by leveraging the well-known solution of the Hill-Clohessy-Wiltshire equations. For small orbit eccentricities, this new model can be used for significantly longer propagation intervals than the commonly used kinematic model. An approach is presented to obtain analytical SNC process noise covariance models for orbital element states for small eccentricities, and then a second approach is presented that is valid for eccentric orbits over small propagation intervals. The developed absolute spacecraft state process noise covariance models are then used to construct process noise covariance models for relative spacecraft states by assuming either small or large interspacecraft separations. However, these frameworks for relative process noise covariance modeling can leverage any absolute process noise covariance model, not just those developed in this paper.

Although the developed process noise covariance models neglect deterministic perturbations in the present work, they are guaranteed positive semi-definite, are much more computationally efficient than numerical solutions, and are more accurate than the commonly used kinematic model for Cartesian states. Numerical simulations show the orbital element models are valid for larger eccentricities and longer propagation intervals than the Cartesian models. Moreover, the small separation relative orbital element model is accurate for larger interspacecraft separations than the small separation relative Cartesian model. Since the orbital element models tend to outperform the Cartesian models, modeling the process noise covariance of Cartesian states through a linear mapping of orbital element models to Cartesian space should be investigated. As future work, it is also important to quantify the degradation of the developed models due to perturbations and to extend the models to long propagation intervals for perturbed and eccentric orbits. In particular, the Cartesian models can potentially be extended to long propagation intervals for eccentric orbits by leveraging the existing solutions of the Tschauner-Hempel equations.[26] Analytical models of the effects of perturbations on orbital elements may possibly be used to improve the presented orbital element process noise covariance models to incorporate perturbations.[14,15] Finally, the use of the recently developed adaptive state noise com-

pensation algorithm should be explored to tune the power spectral density matrix online for these new process noise covariance models.[27]

APPENDIX A: GAUSS VARIATIONAL EQUATIONS

The Gauss Variational Equations are formulated in equinoctial elements by Battin[25] and are provided here for reference. The parameters in Eq. (45) are

$$
\begin{aligned}
\bar{A} &= \frac{2a^2}{\hbar}(f\sin l - g\cos l) & \bar{B} &= \frac{2a^2 W}{\hbar} & \bar{C} &= \sqrt{\frac{p}{\mu}}\sin l \\
\bar{D} &= \sqrt{\frac{p}{\mu}}\frac{f + (1+W)\cos l}{W} & \bar{E} &= \sqrt{\frac{p}{\mu}}\frac{g(k\cos l - h\sin l)}{W} & \bar{F} &= -\sqrt{\frac{p}{\mu}}\cos l \\
\bar{G} &= \sqrt{\frac{p}{\mu}}\frac{g + (1+W)\sin l}{W} & \bar{H} &= \sqrt{\frac{p}{\mu}}\frac{f(h\sin l - k\cos l)}{W} & \bar{I} &= \sqrt{\frac{p}{\mu}}\frac{(1+h^2+k^2)\cos l}{2W} \\
\bar{J} &= \sqrt{\frac{p}{\mu}}\frac{(1+h^2+k^2)\sin l}{2W} & \bar{K} &= -\sqrt{\frac{p}{\mu}}\left(\frac{W-1}{1+\eta} + \frac{2\eta}{W}\right) & \bar{L} &= -\frac{\hbar(1+W)(g\cos l - f\sin l)}{\mu W(1+\eta)} \\
\bar{M} &= -\frac{\hbar(k\cos l - h\sin l)}{\mu W} & W &= 1 + f\cos l + g\sin l & \eta &= \sqrt{1-e^2}
\end{aligned}
\tag{81}
$$

ACKNOWLEDGMENTS

This material is based upon work supported by the National Science Foundation Graduate Research Fellowship Program under Grant No. DGE-1656518. Any opinions, findings, and conclusions or recommendations expressed in this material are those of the authors and do not necessarily reflect the views of the National Science Foundation. The authors also wish to thank the Achievement Rewards for College Scientists (ARCS) Foundation for their support. Additionally, this research is part of the Autonomous Nanosatellite Swarming (ANS) Using Radio-Frequency and Optical Navigation project supported by the NASA Small Spacecraft Technology Program cooperative agreement number 80NSSC18M0058.

REFERENCES

[1] F. H. Schlee, C. J. Standish, and N. F. Toda, "Divergence in the Kalman filter," *AIAA Journal*, Vol. 5, June 1967, pp. 1114–1120, 10.2514/3.4146.

[2] R. Mehra, "Approaches to Adaptive Filtering," *IEEE Transactions on Automatic Control*, Vol. 17, Oct. 1972, pp. 693–698, 10.1109/TAC.1972.1100100.

[3] J. Carpenter, C. D'Souza, F. Markley, and R. Zanetti, "Navigation Filter Best Practices," *NASA TR TP-2018-219822*, 2018.

[4] F. Schiemenz, J. Woodburn, V. Coppola, J. Utzmann, and H. Kayal, "Improved Orbit Gravity Error Covariance for Orbit Determination," *Journal of Guidance, Control, and Dynamics*, Vol. 43, July 2020, pp. 1671–1687. Publisher: American Institute of Aeronautics and Astronautics, 10.2514/1.G004918.

[5] J. Wright, "Sequential Orbit Determination with Auto-Correlated Gravity Modeling Errors," *Journal of Guidance and Control*, Vol. 4, May 1981, pp. 304–309, 10.2514/3.56083.

[6] J. Sullivan, *Nonlinear Angles-Only Orbit Estimation for Autonomous Distributed Space Systems*. PhD thesis, Stanford University, 2020.

[7] B. Schutz, B. Tapley, and G. H. Born, *Statistical Orbit Determination*, pp. 220–233, 499–509. Elsevier, 2004, ISBN:978-0-08-054173-0.

[8] G. J. Bierman, *Factorization Methods for Discrete Sequential Estimation*, pp. 150–152. Academic Press, Inc., 1977.

[9] J. M. Leonard, F. G. Nievinski, and G. H. Born, "Gravity Error Compensation Using Second-Order Gauss-Markov Processes," *Journal of Spacecraft and Rockets*, Vol. 50, Jan. 2013, pp. 217–229, 10.2514/1.A32262.

[10] K. A. Myers and B. D. Tapley, "Dynamical Model Compensation for Near-Earth Satellite Orbit Determination," *AIAA Journal*, Vol. 13, No. 3, 1975, pp. 343–349, 10.2514/3.49702.

[11] B. Tapley and D. Ingram, "Orbit Determination in the Presence of Unmodeled Accelerations," *IEEE Transactions on Automatic Control*, Vol. 18, Aug. 1973, 10.1109/TAC.1973.1100331.

[12] D. B. Goldstein, G. H. Born, and P. Axelrad, "Real-Time, Autonomous, Precise Orbit Determination Using GPS," *Navigation*, Vol. 48, No. 3, 2001, pp. 155–168, 10.1002/j.2161-4296.2001.tb00239.x.

[13] J. Sullivan, T. Lovell, and S. D'Amico, "Angles-Only Navigation for Autonomous On-Orbit Space Situational Awareness Applications," *2018 AAS/AIAA Astrodynamics Specialist Conference*, Snowbird, UT, 2018.

[14] T. Guffanti and S. D'Amico, "Linear Models for Spacecraft Relative Motion Perturbed by Solar Radiation Pressure," *Journal of Guidance, Control, and Dynamics*, Vol. 42, Apr. 2019, pp. 1962–1981, 10.2514/1.G002822.

[15] A. W. Koenig, T. Guffanti, and S. D'Amico, "New State Transition Matrices for Spacecraft Relative Motion in Perturbed Orbits," *Journal of Guidance, Control, and Dynamics*, Vol. 40, No. 7, 2017, pp. 1749–1768, 10.2514/1.G002409.

[16] G. R. Hintz, "Survey of Orbit Element Sets," *Journal of Guidance, Control, and Dynamics*, Vol. 31, No. 3, 2008, pp. 785–790. Publisher: American Institute of Aeronautics and Astronautics _eprint: https://doi.org/10.2514/1.32237, 10.2514/1.32237.

[17] J. Sullivan, S. Grimberg, and S. D'Amico, "Comprehensive Survey and Assessment of Spacecraft Relative Motion Dynamics Models," *Journal of Guidance, Control, and Dynamics*, Vol. 40, No. 8, 2017, pp. 1837–1859. Publisher: American Institute of Aeronautics and Astronautics _eprint: https://doi.org/10.2514/1.G002309, 10.2514/1.G002309.

[18] K. A. Myers, *Filtering Theory Methods and Applications to the Orbit Determination Problem for Near-Earth Satellites*. PhD thesis, The University of Texas at Austin, 1974.

[19] Y. Bar-Shalom, X.-R. Li, and T. Kirubarajan, *Estimation with Applications to Tracking and Navigation*, ch. 6, pp. 269–270. John Wiley and Sons, Ltd, 2002, 10.1002/0471221279.

[20] W. H. Clohessy and R. S. Wiltshire, "Terminal Guidance System for Satellite Rendezvous," *Journal of the Aerospace Sciences*, Vol. 27, No. 9, 1960, pp. 653–658, 10.2514/8.8704.

[21] K. Alfriend, S. Vadali, P. Gurfil, J. How, and L. Breger, *Spacecraft Formation Flying*, pp. 84–86,99–103. Elsevier, 2010.

[22] F. D. Brujin, E. Gill, and J. How, "Comparative Analysis of Cartesian and Curvilinear Clohessy-Wiltshire Equations," *Journal of Aerospace Engineering, Sciences and Applications*, Vol. 3, No. 2, 2011, pp. 1–15, 10.7446/jaesa.

[23] D. K. Geller, "Orbital Rendezvous: When is Autonomy Required?," *Journal of Guidance, Control, and Dynamics*, Vol. 30, July 2007, pp. 974–981, 10.2514/1.27052.

[24] M. Willis, K. T. Alfriend, and S. D'Amico, "Second-Order Solution for Relative Motion on Eccentric Orbits in Curvilinear Coordinates," *2019 AAS/AIAA Astrodynamics Specialist Conference*, Portland, ME, 2019.

[25] R. H. Battin, *An Introduction to the Mathmatics and Methods of Astrodynamics*, pp. 490–493. AIAA, 1987.

[26] K. Yamanaka and F. Ankersen, "New State Transition Matrix for Relative Motion on an Arbitrary Elliptical Orbit," *Journal of Guidance, Control, and Dynamics*, Vol. 25, Jan. 2002, pp. 60–66, 10.2514/2.4875.

[27] N. Stacey and S. D'Amico, "Adaptive and Dynamically Constrained Process Noise Estimation for Orbit Determination," *IEEE Transactions on Aerospace and Electronic Systems*, 2021.